

PAPER • OPEN ACCESS

Development of a high current density, high temperature superconducting cable for pulsed magnets

To cite this article: Charlie Sanabria *et al* 2024 *Supercond. Sci. Technol.* **37** 115010

View the [article online](#) for updates and enhancements.

You may also like

- [Natural width of the superconducting transition in epitaxial TiN films](#)
Elmira Baeva, Anna Kolbatova, Nadezhda Titova *et al.*
- [Effect of substrate temperature on the growth mechanism of FeSe superconducting films](#)
Ya-Xun He, Jia-Ying Zhang, Tian He *et al.*
- [A high throughput facility for the RF characterisation of planar superconducting thin films](#)
D Seal, O B Malyshev, P Goudket *et al.*

Development of a high current density, high temperature superconducting cable for pulsed magnets

Charlie Sanabria^{1,*}, Alexey Radovinsky¹, Christopher Craighill¹, Kiran Uppalapati¹, Alex Warner¹, Julio Colque¹, Elle Allen¹, Sera Evcimen¹, Sam Heller¹, David Chavarria¹, Kristen Metcalfe¹, Saehan Lenzen¹, Amanda Hubbard², Amy Watterson², Sarah Chamberlain², Rui Diaz-Pacheco¹, Benjamin Weinreb¹, Elizabeth Brownell¹, Justin Nealey¹, Annie Hughes¹, Eric Laamanen¹, Keshav Vasudeva¹, Daniel Nash¹, Colin McCormack¹, Erica Salazar¹, Owen Duke¹, Matt Hicks¹, Jeremy Adams¹, Dylan Kolb-Bond¹, Timothy Liu¹, Kara Malhotra¹, David P Meichle¹, Ashleigh Francis¹, JL Cheng¹, Maise Shepard¹, Aliya Greenberg¹, Vinny Fry¹, Nick Kostifakis¹, Carl Avola¹, Paul Ljubicic¹, Lex Palmer¹, Gayatri Sundar Rajan¹, Ronak Padukone¹, Sergey Kuznetsov¹, Kai Donez¹, Theodore Golfinopoulos², Philip C Michael², Rui Vieira², Nicolai Martovetsky³, Rodney Badcock⁴, Mike Davies⁴, Arvid Hunze⁴, Bart Ludbrook⁴, Ramesh Gupta⁵, Piyush Joshi⁵, Shresht Joshi⁵, Anis Ben Yahia⁵, Hugo Bajas⁶, Markus Jenni⁶, Christoph Mueller⁶, Manuel Holenstein⁶, Kamil Sedlak⁶, Brandon Sorbom¹ and Daniel Brunner¹

¹ Commonwealth Fusion Systems, Devens, MA, United States of America

² Plasma Science and Fusion Center, Massachusetts Institute of Technology, Cambridge, MA, United States of America

³ Oak Ridge National Laboratory, Oak Ridge, TN, United States of America

⁴ Paihau-Robinson Research Institute, Victoria University of Wellington, Wellington, New Zealand

⁵ Brookhaven National Laboratory, Upton, NY, United States of America

⁶ Ecole Polytechnique Federale de Lausanne Swiss Plasma Center, Lausanne, Vaud, Switzerland

E-mail: charlie@cfs.energy

Received 24 January 2024, revised 16 September 2024

Accepted for publication 24 September 2024

Published 4 October 2024



Abstract

A low-AC loss Rare-earth barium copper oxide (REBCO) cable, based on the VIPER cable technology has been developed by commonwealth fusion systems for use in high-field, compact tokamaks. The new cable is composed of partitioned and transposed copper ‘petals’ shaped to fit together in a circular pattern with each petal containing a REBCO tape stack and insulated from each other to reduce AC losses. A stainless-steel jacket adds mechanical robustness—also serving as a vessel for solder impregnation—while a tube runs through the middle for cooling purposes. Additionally, fiber optic sensors are placed under the tape stacks for quench detection (QD). To qualify this design, a series of experiments were conducted as part of the SPARC tokamak central solenoid (CS) model coil program—to retire the risks associated with full-scale, fast-ramping, high-flux high temperature superconductors CS and poloidal field coils for tokamak fusion power plants and net-energy demonstrators. These risk-study and

* Author to whom any correspondence should be addressed.



Original content from this work may be used under the terms of the [Creative Commons Attribution 4.0 licence](#). Any further distribution of this work must maintain attribution to the author(s) and the title of the work, journal citation and DOI.

risk-reduction experiments include (1) AC loss measurement and model validation in the range of $\sim 5 \text{ T s}^{-1}$, (2) an IxB electromagnetic (EM) loading of over 850 kN m^{-1} at the cable level and up to 300 kN m^{-1} at the stack level, (3) a transverse compression resilience of over 350 MPa, (4) manufacturability at tokamak-relevant speeds and scales, (5) cable-to-cable joint performance, (6) fiber optic-based QD speed, accuracy, and feasibility, and (7) overall winding pack integration and magnet assembly. The result is a cable technology, now referred to as PIT VIPER, with AC losses that measure fifteen times lower (at $\sim 5 \text{ T s}^{-1}$) than its predecessor technology; a 2% or lower degradation of critical current (I_c) at high IxB EM loads; no detectable I_c degradation up to 600 MPa of transverse compression on the cable unit cell; end-to-end magnet manufacturing, consistently producing I_c values within 7% of the model prediction; cable-to-cable joint resistances at 20 K on the order of $\sim 15 \text{ n}\Omega$; and fast, functional QD capabilities that do not involve voltage taps.

Keywords: fusion energy, tokamak, REBCO, cable, novel, pulsed magnets, compact

1. Introduction

The SPARC fusion device—currently under construction in Devens, Massachusetts by Commonwealth Fusion Systems (CFS) in collaboration with the MIT Plasma Science and Fusion Center (PSFC)—is a high-field tokamak with $\sim 20 \text{ T}$ on-coil [1], designed to operate at a performance range made possible thanks to the continued improvement of Rare-earth barium copper oxide (REBCO) high temperature superconductors (HTS) over the past two decades [2–5]. Similarly, the significant scale-up in production of REBCO HTS tapes in recent years [6–8], driven by fusion energy initiatives from both the private sector and government agencies [9–11], has made SPARC’s construction an attainable reality. This demonstration device is a significant milestone for CFS’ mission to put fusion power on the grid by mid 2030s, using a serviceable power plant called ARC [12].

A pulsed tokamak such as SPARC (and eventually ARC) requires robust, high-field, and low-loss central solenoid (CS) and poloidal Field (PF) coils to initiate, drive, and shape the plasma. Such coils pose significant challenges at the conductor level to balance the needs for low AC losses, high current capacity, cooling capacity, mechanical robustness, and quench detection (QD) capabilities. CFS and MIT in 2018–2020 developed a REBCO cable technology called VIPER (an acronym derived from its manufacturing steps [13])—based on the twisted stack tape cable approach [14]—which was studied in parallel with the No-Insulation No-Twist (NINT) concept to consider its use in a high-field, steady-state demonstration magnet for fusion relevant toroidal field (TF) coils [15–17]. This TF Model Coil project ultimately selected a NINT architecture, but VIPER cables were still used for its current feeder lines. VIPER may also be used for stellarator coils [18], or any other steady-state magnet operating in the 20 K and 50 kA range. However, given that the VIPER cable was not optimized for fast ramping applications such as the CS or PF coils in a tokamak, CFS started in 2019 to develop a low-AC loss REBCO cable for the CS and PF coils of SPARC, aided by the Advanced Research Projects Agency-Energy (ARPA-E) program of the US Department of Energy.

The goal of this ARPA-E grant was to retire the key risks associated with pulsed magnets for high field tokamaks using a 2nd generation VIPER cable and to prove the technology readiness via a demonstration magnet; a central solenoid model coil (CSMC). The purpose of this paper is to focus on this emerging low-AC loss HTS technology, and the various experiments designed to retire some of the key risks of SPARC CS and PF coils.

SPARC was designed with an on-axis TF, B_0 , of 12.2 T with a peak field in the winding pack of 25 T. One of the unique features of SPARC is the use of no-insulation technology for the steady state magnets of the TF magnet system, a technology that has been rigorously de-risked by CFS and the PSFC—at SPARC-relevant scales—including the construction and testing of a toroidal field model coil (TFMC) [15]. Other magnet systems of a tokamak, such as the CS and PF coils are pulsed magnets where a no-insulation approach is not practical due to the fast charge rate required in these magnets during plasma operation. A sketch highlighting the pulsed magnet systems in SPARC is shown in figure 1 and the main parameters are shown in table 1.

One of the most challenging features of these coils is the high ramp-rates required to produce 42 Wb of magnetic flux in a very small volume to initiate and drive the plasma current—which can put the inner layer of the CS at field ramp rates as high as 4.6 T s^{-1} . To achieve this, it was necessary to redesign the VIPER conductor to reduce its AC losses.

2. Reducing AC losses in VIPER cables

Changing the magnetic field in an electromagnet induces heating within the magnet; the different phenomena inducing heating are often lumped together in the term ‘AC losses’. For fast ramping fields—e.g. a few available at: as in the SPARC and ARC CS—the heating due to AC losses can be a major design driver and limiter of magnet performance. These losses can be grouped into three main groups: eddy current losses, coupling losses, and hysteretic losses [19]. Given that hysteretic losses are an inherent phenomena of the superconductor, it

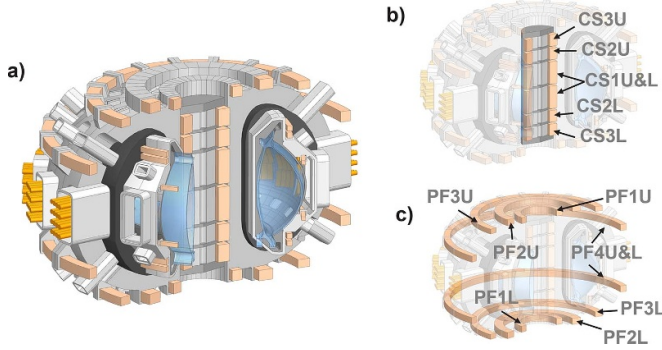


Figure 1. Conceptual renderings of SPARC. (a) overview, (b) central solenoid highlighted showing the module numbering from the mid-plane outwards with upper/lower symmetry, and (c) poloidal field coils highlighted showing the module numbering (outwards-in) with upper/lower symmetry. Image courtesy of Trey Henderson III.

Table 1. Principal parameters and description of the CS and PF magnet systems of SPARC.

Parameter and units	CS	PF
Modules, description	Three upper and three lower coils, all independently powered. Upper and lower are symmetric (see figure 1)	Four upper and four lower coils, all independently powered. Upper and lower are symmetric (see figure 1)
Module 1 inner radius/outer radius/height, m	0.445/0.695/0.984	0.79/1.05/0.269
Module 2 inner radius/outer radius/height, m	0.454/0.695/0.472	1.468/1.832/0.269
Module 3 inner radius/outer radius/height, m	0.454/0.695/0.472	2.494/2.806/0.215
Module 4 inner radius/outer radius/height, m	—	3.72/3.98/0.323
Longest continuous cable length, m	163	241
Shortest continuous cable length, m	50.3	57.8
Total cable length required (full system), km	13.7	5.1
Peak stored energy (full system), MJ	886	409
Module 1 peak field, T	25	10.1
Module 2 peak field, T	18	7.6
Module 3 peak field, T	16	7.5
Module 4 peak field, T	—	6.9
Engineering current density at peak field, A mm ⁻²	113	69
Peak ramp rate during plasma drive, T/s	4.6	1.8
Average winding pack stress expected at peak field (CS and TF on), MPa	−180 ^a	150
Average winding pack stress expected (CS off, TF on), MPa	−240 ^a	0
Operating temperature range, K	15–30	15–30
Cooling, description	2 g s ^{−1} He gas at 20 bar	2.5 g s ^{−1} He gas at 20 bar
Winding style	Layer	Pancake

^a Even at peak field, the CS of SPARC finds itself under compression due to TF loads (more on section 5).

was deemed impractical for the SPARC project to attempt to reduce hysteretic losses via modifications of the HTS tape geometry [20–22], provided the schedule constraints and the cost & scale needs for CFS' mission. Therefore, it was decided to use 4 mm wide tape without any hysteretic loss mitigation strategies since the hysteretic contribution calculated from literature values [23, 24] was deemed acceptable compared to eddy and coupling losses of VIPER. Another design constraint that affects the ability to reduce AC losses has to do with the principle of a soldered twisted stack which is responsible for VIPER's success [15]. Therefore, any new cable designs must remain a soldered twisted-stack tape conductor to obtain similar performance metrics and must use 4 mm-wide tapes for scalability. These constraints leave us with one main lever to

reduce AC losses: partitioning the copper to minimize eddy currents. This design change (a partitioned former) is now differentiated by a simple acronym added to the original name: now dubbed PIT VIPER, or, partitionally insulated and transposed VIPER cable, proposed in late 2019 [25]. The main change is the addition of electrical insulation on all faces of the former 'petals' except those facing the HTS tape-stack (see figure 2). Just like VIPER, it can be made of virtually any number of stacks with as many HTS tapes per stack as the copper former dimension allows (roughly between 60 and 100 HTS tapes per stack depending on the tape thickness). A cross section of the PIT VIPER cable is shown in figure 2. A similar concept (SECAS cable [26]) has recently been proposed, albeit with significant manufacturing and operational differences.

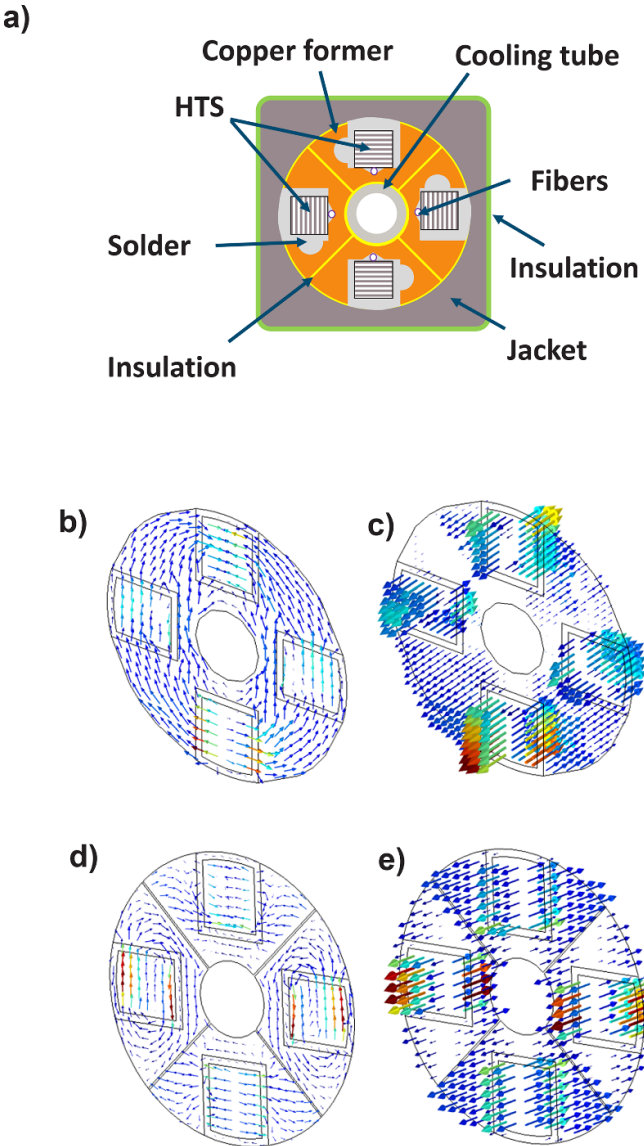


Figure 2. (a) cross section of a PIT VIPER cable with a square jacket and a stainless-steel cooling tube. (b) and (c) planar and axial arrow plots of eddy current patterns generated in VIPER. (d) and (e) planar and axial arrow plots of eddy current patterns generated in PIT VIPER under a uniform ramping magnetic field. Current arrows are modeled using COMSOL multiphysics.

To qualify PIT VIPER for SPARC use, several risks must be retired in addition to what was done for VIPER:

- Risk 1: the high AC losses observed in most REBCO conductors [23, 24, 27, 28] causes localized overheating and quenches the magnets during operation.
- Risk 2: the high $I_{\text{c}}B$ load acting on a partitioned cable causes damage to HTS and reduces performance past operational I_{c} limits. This risk has proven very challenging for other REBCO based cables [29, 30] proposed for fusion devices.
- Risk 3: high compressive loads on the CS cause irreversible (plastic) structural damage or component failure to the

CS (e.g. HTS, fiber optics, or insulation failure). This compressive load is a result of the enormous centering forces that attract all TF coils to the center of the tokamak. In SPARC, this load is supported at the CS-TF interface. Such a design is referred to as a ‘bucked’ tokamak which puts the CS in compression—as opposed to a ‘wedged’ tokamak (e.g. ITER) in which the force is reacted at the TF-TF interface and the CS is self-supporting.

- Risk 4: manufacturability of long lengths. There are many REBCO cable technologies that have not moved past their conceptual stages [21, 31, 32].
- Risk 5: high joint resistances or high joint AC losses cause premature quenches during operation.
- Risk 6: QD system is not robust enough to prevent coil damage during quench events, given the slow quench propagation velocity of HTS conductors [33].
- Risk 7: integration and testing of a fully manufactured magnet. This encompasses many risks which are inherent to every magnet system such as insulation defects [34], unexpected heat loads [35], weldment issues [36], quench protection failures [37], lead/joint connection issues [38], operator error [39, 40], etc.

Over the next few sections of this manuscript, we will visit the R&D designed to address each risk, their results, and follow-up requirements (if any).

3. Risk 1: high AC loss observed in most REBCO conductors to date

AC losses in superconductors manifest themselves in a wide range of intensities across different regimes and configurations [19]. While modeling is a critical tool in assessing the AC losses of a superconducting cable design, it is hard to capture all the details of the physics involved. Experiments are necessary to validate model results. This has led to practical characterization methods via sinusoidal field fluctuations across a range of frequencies (with a limited amplitude) at different background fields [41]—often done with and without current to understand the effects of transport current on the losses. Such experiments require well-established wire/cable geometries and a significant characterization campaign at all stages and operating regimes of the conductor.

At the time of the PIT VIPER conception (late 2019) and given project schedule constraints (four years to build a demonstration magnet), it was not feasible to fully characterize PIT VIPER cables comprehensively in a matter of a few months, since it would have required several meters of cable and a rigorous testing campaign at a magnet such as SULTAN. Even if such a campaign were launched, it would have been limited by low field sweep amplitudes ($<1 \text{ T s}^{-1}$ in practice) and currents below the full capacity of PIT VIPER [42]. Instead, our initial experiments focused on proof-of-concept by measuring the losses in short samples without transport current (i.e. not electrically connected to the magnet producing the background field). The losses were measured

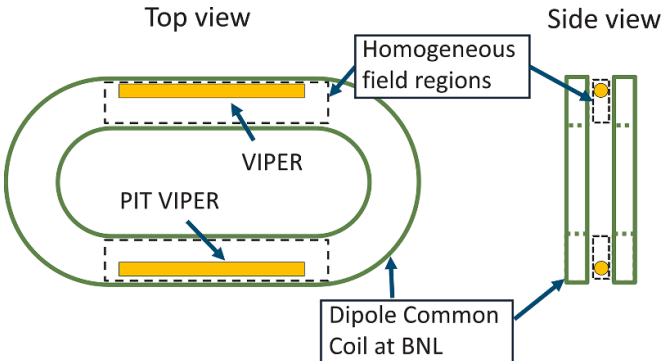


Figure 3. Experimental setup and sample position with respect to the dipole common coil at BNL. The stainless-steel vacuum vessels (insulating the samples) are not shown.

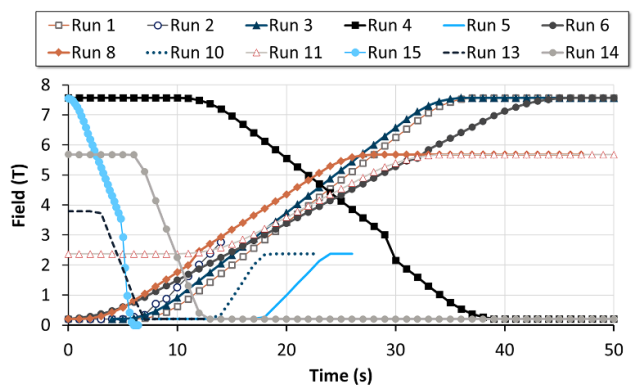
via calorimetry on 280 mm-long VIPER and PIT VIPER cable sections having four full-HTS stacks (with a twist pitch of 200 mm) under ramping magnetic fields induced by the Dipole Common Coil at the Brookhaven National Laboratory (BNL) [43], see figure 3. All dimensions and components are identical in these two samples except the partitions of the PIT VIPER cables. The samples were fully encased in stainless-steel vacuum vessels, insulated (electrically and thermally) at their contact points using G-10 supports. Three cernox sensors per sample were anchored to exposed sections of copper former along the length and their wires routed (in vacuum) to room temperature via Klein Flansche feedthroughs with multi-pin D-sub connectors. The experiment includes linear ramps between 0.2 T s^{-1} and 0.9 T s^{-1} and magnet fast-discharges (of the common coil) which induce field ramp rates on the samples of up to -30 T s^{-1} . During the ramps and discharges, the temperature rise was measured using three cernox sensors along the length to assess the AC losses of each run via calorimetry. The magnet was energized or de-energized with the parameters shown in table 2 and figure 4. A typical run and the evolution of field and temperature are shown in figure 5

The heat generated on the sample is calculated using the instantaneous heat capacity, the sample mass, and the change in temperature measured. The three cernox sensor values are averaged to obtain the sample temperature. The recorded temperature does not show any gradients higher than 1 K during a particular run, and the temperature within the cable cross section is assumed uniform. To illustrate the nature of the losses observed, the heat traces for runs with *low, positive* $\text{d}B/\text{dt}$ are shown in figure 6. It is evident that PIT VIPER shows negligible changes in its loss profile with small changes in $\text{d}B/\text{dt}$, while VIPER fluctuates much more drastically. Given that eddy and coupling losses are strongly dependent on $\text{d}B/\text{dt}$ while hysteresis are B dependent, it is likely that *at these low ramp rates* the losses in PIT VIPER are largely hysteretic in nature while the losses in VIPER are dominated by eddy and coupling currents. This nonlinear evolution of the heat generation observed for PIT VIPER in figure 6 further reinforces the hysteretic-dominant hypothesis, given that hysteretic losses

Table 2. Peak field and target ramp rates generated by the common coil magnet for the runs analyzed.

Run number	Description	Peak field (T)	Target $\text{d}B/\text{dt}$ (T/s)
Run 1	Ramp	7.57	0.28
Run 2	Ramp	2.76	0.38
Run 3	Ramp	7.57	0.28
Run 4	Ramp	7.57	-0.28
Run 5	Ramp	2.38	0.38
Run 6	Ramp	7.57	0.19
Run 7	Fast dump	7.57	≈ -30 (see figure 4(b))
Run 8	Ramp	5.68	0.24
Run 9	Fast dump	5.68	≈ -9 (see figure 4(b))
Run 10	Ramp	2.37	0.56
Run 11	Ramp	5.68	0.19
Run 12	Fast dump	5.68	≈ -18 (see figure 4(b))
Run 13	Ramp	3.79	-0.94
Run 14	Ramp	5.68	-0.94
Run 15	Ramp & quench	7.57	≈ -2.7 (see figure 4(a))

a)



b)

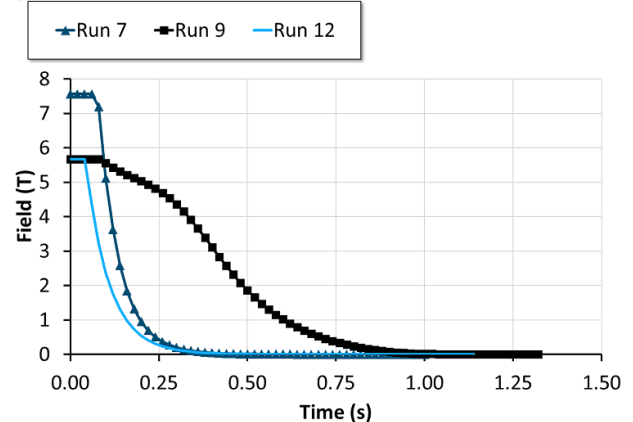


Figure 4. Field as a function of time for the runs analyzed (a) linear ramps (b) magnet quenches.

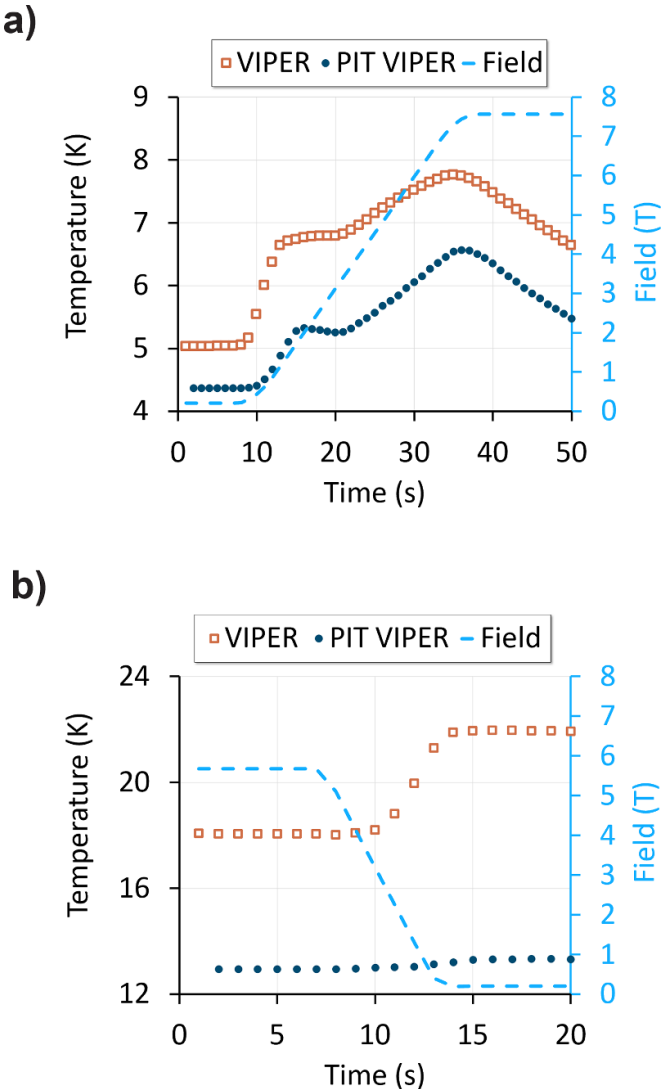


Figure 5. Field and sample temperature traces for (a) Run 1 at 0.28 T s^{-1} and (b) Run 14 at -0.94 T s^{-1} . The drop in temperature observed in Run 1 after the run is complete is due to an increase in pressure (accidental helium leak) in the sample vessels during this run.

are dependent on B^3 below a certain penetration field, while linear above it—putting the penetration field for twisted tape stacks somewhere between 1 T and 2 T, a middle ground from those measured in [23] and [44].

Using the rate of change in temperature (and therefore in heat generated), the instantaneous power in W/m can be calculated and plotted as a function of dB/dt as shown in figure 7. The trend shown (a simple exponential fit in log scale) reveals a significant reduction in losses across a wide variety of ramp rates for the PIT VIPER sample, which corresponds to a reduction of roughly 15 times at $\sim 5 \text{ T s}^{-1}$.

COMSOL multiphysics models with reasonable experimental agreement are shown in figure 8. These models are currently ignoring hysteretic losses, and therefore the exact

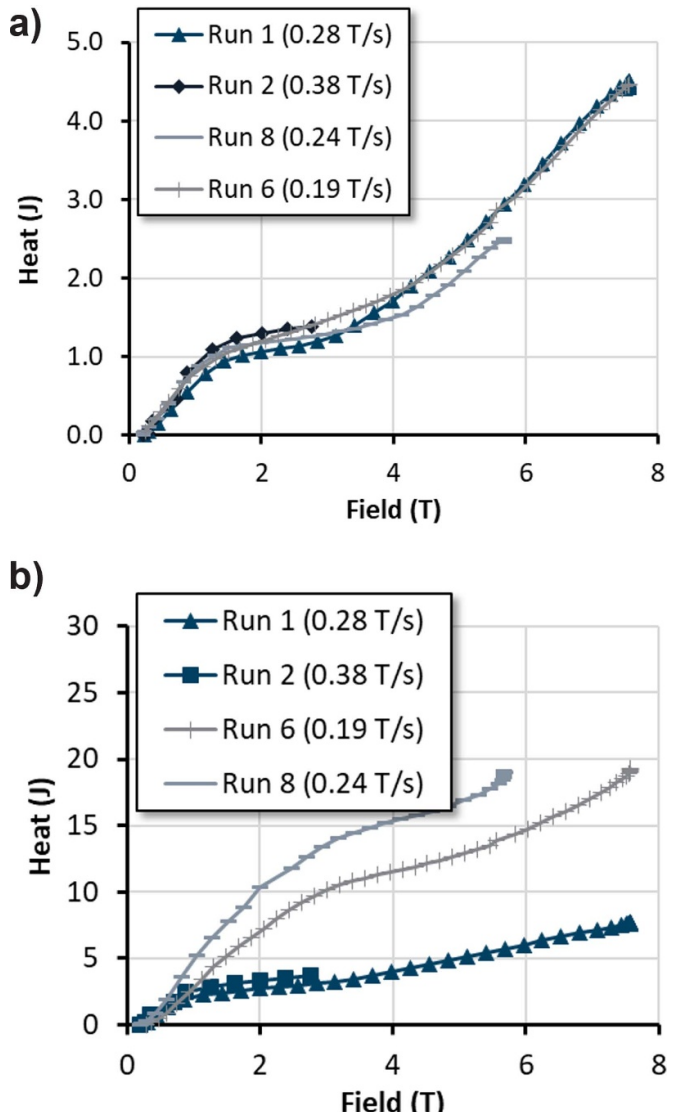


Figure 6. Heat generated at low, positive dB/dt runs for (a) the PIT VIPER sample and (b) the VIPER sample; note the difference in vertical scales and lower heating in the PIT VIPER sample.

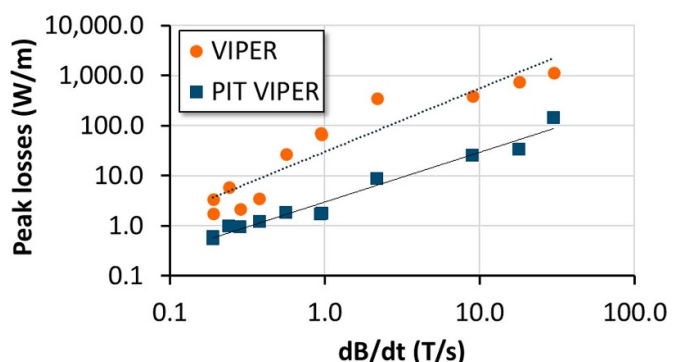


Figure 7. Peak losses in W/m for all the runs as a function of ramp-rate for both VIPER and PIT VIPER samples.

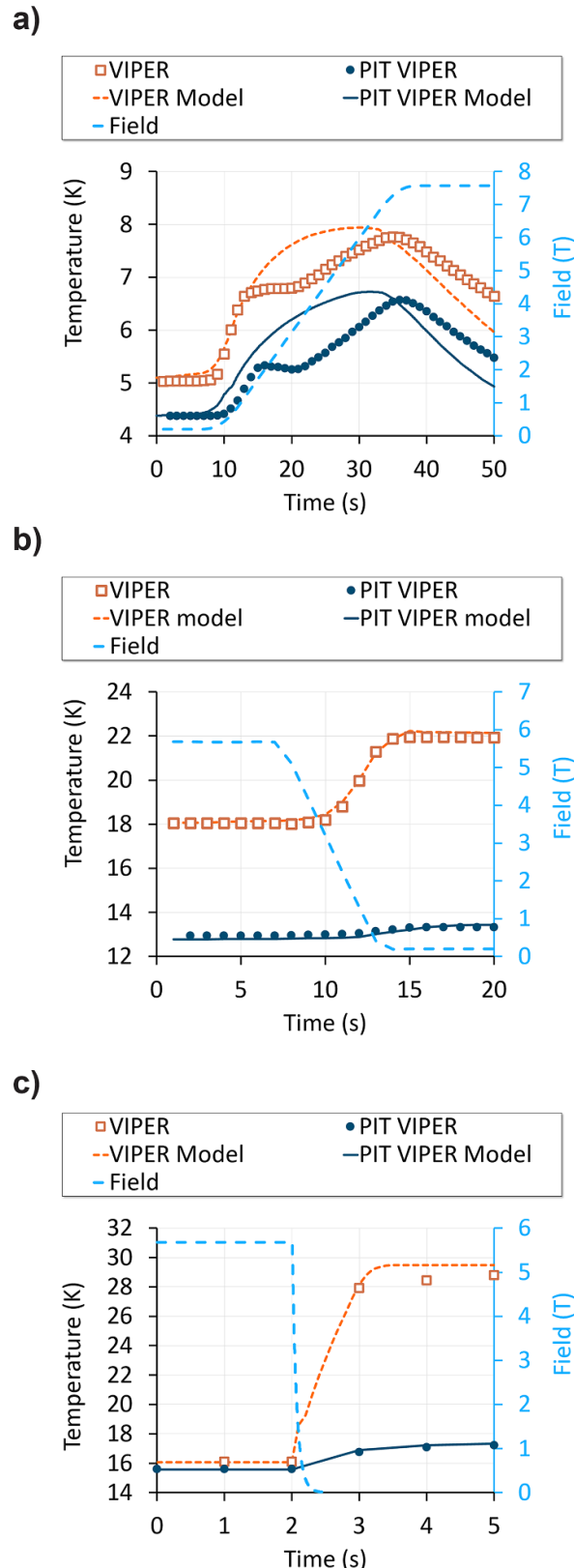


Figure 8. Peak field and average sample temperature values obtained from COMSOL multiphysics models of the full cable pieces inside the common coil gradient for (a) Run 1, (b) Run 14, and (c) Run 9. Models ignore hysteresis. The drop in temperature observed in Run 1 after the run is complete is due to poor vacuum during that run, resulting in higher convection to the he bath outside the sample vacuum vessels. The cooling power as a function of temperature for Run 1 was derived from the temperature traces and added to the model.

temperature traces are much more difficult to capture for low dB/dt runs. Nonetheless, at the most relevant ramp-rate values ($>1 \text{ T s}^{-1}$), these models still provide very good estimates of the total losses. Hysteretic models and higher field measurements are important follow-up experiments currently under development.

The initial approximation of these losses in a fast-turnaround experiment (conceived in July 2020 and results obtained four months later), combined with the validation of models at high dB/dt , provided the required information to proceed with the de-risking of PIT VIPER for SPARC (and even ARC) as shown below, without having to increase the cooling scheme, make significant cable design changes, or modify the tape-stack configuration. Henceforth, the design of the PIT VIPER cable-in-conduit conductor (CICC) was locked in. Twist pitch, tape stack size, cooling tube dimensions, and copper fraction were fixed. Only the number of petals (four or five) and/or the number of HTS tapes within that petal were altered to increase or decrease the transport current by adding or removing filler or ‘dummy’ tapes made of stainless steel. This ability to change critical current of a particular sample by modifying the number of HTS tapes and replacing a mechanically equivalent filler tape, allowed us to tailor the cable designs for a particular risk-retirement experiment—without having to utilize all the HTS real estate.

To predict critical current density of the cables, we used the electrical models described in appendix A combined with the tape data up to 20 T acquired using the methods outlined in appendix B. Such models seem to predict the cable performance with reasonable margin of error (likely coming from manufacturing processes as it will be discussed in section 6 of this manuscript). Mechanically, we have assumed that the petals act independently under lorentz loads, an assumption that has proven reasonable on these and other experiments of soldered tape stacks inside a copper former [13, 18, 45]. Under external loads, the monolithic nature of the soldered cable also appears to generate similar stress-strain conditions within the tape stack with either four or five-petal cables (see appendix C). Occasionally, for ease of manufacturing and in cases where external load was not applied, the jacket (or conduit) shape was altered from circle-in-square to a round jacket. Hence, the experiments presented in this manuscript have just enough HTS tapes to obtain the necessary data to retire each risk; be it I_c degradation due to electromagnetic (EM) loads, external loads, manufacturing processes, etc., or to reach a particular operational state, such as is required for QD.

4. Risk 2: high I_{xB} loading of a high field magnet

At peak loading conditions of SPARC CS, 50 kA and 25 T, the transverse I_{xB} load at the innermost layer (which has a 5-petal cable) reaches 250 kN m^{-1} per stack. The performance of VIPER cables had already been qualified in 2019 to similar loads with acceptably low degradation of I_c , in the order of a few percent [13]. These experiments use a single HTS petal under the assumption that the petals are sufficiently

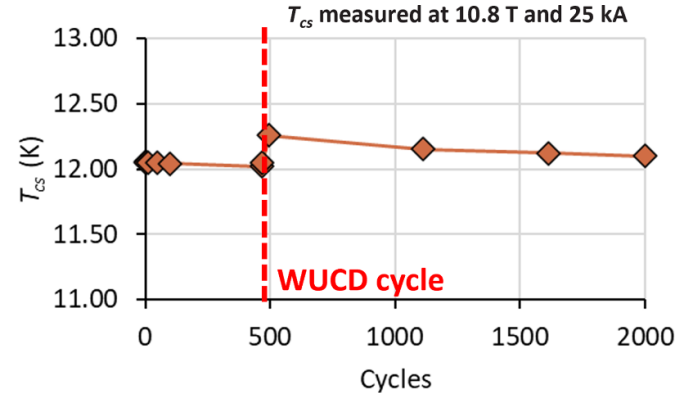


Figure 9. T_{cs} evolution of a PIT VIPER sample having a single tape-stack of HTS loaded at 300 kN m^{-1} for 2000 cycles showing very little performance degradation which should be equivalent during SPARC conditions at higher temperatures with higher tape counts.

independent to retire the internal (I_{xB}) forces of the cable (a reasonable assumption given the monolithic nature of the cable and as long as there is no bending, as is required for SULTAN tests). However, the partitions of PIT VIPER were different enough structurally that a re-qualification was warranted to retire the new I_{xB} load risk and to confirm that the petals are still independent. To do so, a three-meter-long PIT VIPER sample with a single HTS tape stack (and filler non-HTS tape stacks in the other petals) was tested at the SULTAN facility [46]. The current sharing temperature, T_{cs} , evolution of this sample under a stack-loading of 300 kN m^{-1} (27.5 kA at 10.9 T) is shown in figure 9, exhibiting a negligible change in T_{cs} after 2000 EM cycles having a slight change during the warmup-cooldown cycle. These results confirmed that PIT VIPER does not have any disadvantages in its performance compared to VIPER under relevant I_{xB} loads.

The above-mentioned operational parameters of 50 kA, 20 K and 25 T of SPARC CS are expected to be achieved with an I_{op}/I_c of ~ 0.9 for a five-petal cable using the methods described in appendices A and B and using HTS tape with $J_e(B, T, \theta)$ performance already procured for the SPARC project. Hence, this experiment solely focused on studying the stack performance under a particular strain—generated by 300 kN m^{-1} on a single stack. The results indicate that there will be no degradation of performance under these loads.

5. Risk 3: high compressive loads from a bucked design tokamak

The bucked design of SPARC, carrying the TF radial centering loads in the CS, puts the CS winding pack under smeared compressive loads of $\sim 300 \text{ MPa}$ when the TF is on and the CS is off. This *external* load is counteracted when CS is on, but the magnet remains in compression. Finite element analysis (FEA) of PIT VIPER cables in the SPARC CS under peak loading conditions indicate maximum strains on the HTS of -0.4% , which exceeds most values tested in

the literature on unsoldered tapes and cables [47–49], and could surpass the irreversible strain limits of the HTS [50, 51]. Similarly, exceeded allowables are observed in FEA of the winding pack on the turn insulation—a composite layer of E-glass and Kapton having a thickness of 0.5 mm—reaching a tensile strain as high as 5.4% through-thickness, 1% along the glass layers, and shear strains of 4.6%. Two experiments were designed to replicate the peak strain values mentioned above but using a single transverse load at 77 K under liquid nitrogen—allowing for an inexpensive and conservative initial assessment of the risks under compressive loads.

5.1. HTS degradation under transverse compression

The 1st generation VIPER technology was heavily tested under transverse IxB loading and axial tension simultaneously at 10.9 T and below 30 K in 2019 [52], displaying a surprising resilience beyond the experimentally-observed irreversible effects of HTS [50] and far beyond what other similar cable technologies can achieve [29]. However, the loading of the SPARC CS has a hoop *compression* (induced by the bucking TF magnets) which produces a combination of longitudinal and transverse compression on the conductor. This is a very different load case than that seen in most superconducting magnets, never tested in VIPER, and not something that can be tested in a magnet facility with a limited bore size such as SULTAN. To study the effects of this high compressive state on PIT VIPER cables we have relied (so far) on purely transverse loading at 77 K and self-field I_c measurements. A 50 ton hydraulic press was equipped with a ~2 m-long trough containing liquid nitrogen within the press frame, insulated, and adapted with a pusher capable of loading up to 450 MPa over a cable length of 50 mm (or higher if the contact length is reduced). Square-jacketed PIT VIPER samples with a single HTS stack (and dummy tape stacks in the other petals) were prepared and compressed with unconstrained sides for >100 cycles under a peak load of 400 MPa and a minimum load of 200 MPa—with occasional unloaded states for I_c measurements. Three different samples with different orientations of the tape stacks (within their 200 mm twist-pitch spiral) were used at 0°, 45°, and 90° with respect to the force direction as shown in figure 10(a). Voltage tap pairs with 200 mm spacing were used to monitor voltage during I_c curve measurements done in the unloaded condition every few compression cycles.

The results observed in figure 10 indicate no I_c changes beyond a few percent (measurement error) at 400 MPa for over 100 compressive cycles and an onset of irreversible degradation (>5%) is observed only above 650 MPa. CFS is presently investigating the effects of a longitudinal compression combined with transverse to further investigate the loading conditions in SPARC with very encouraging results [45].

5.2. Insulation integrity under transverse compression

To investigate the effects on turn insulation under these load conditions, an array of cables is necessary. Similar

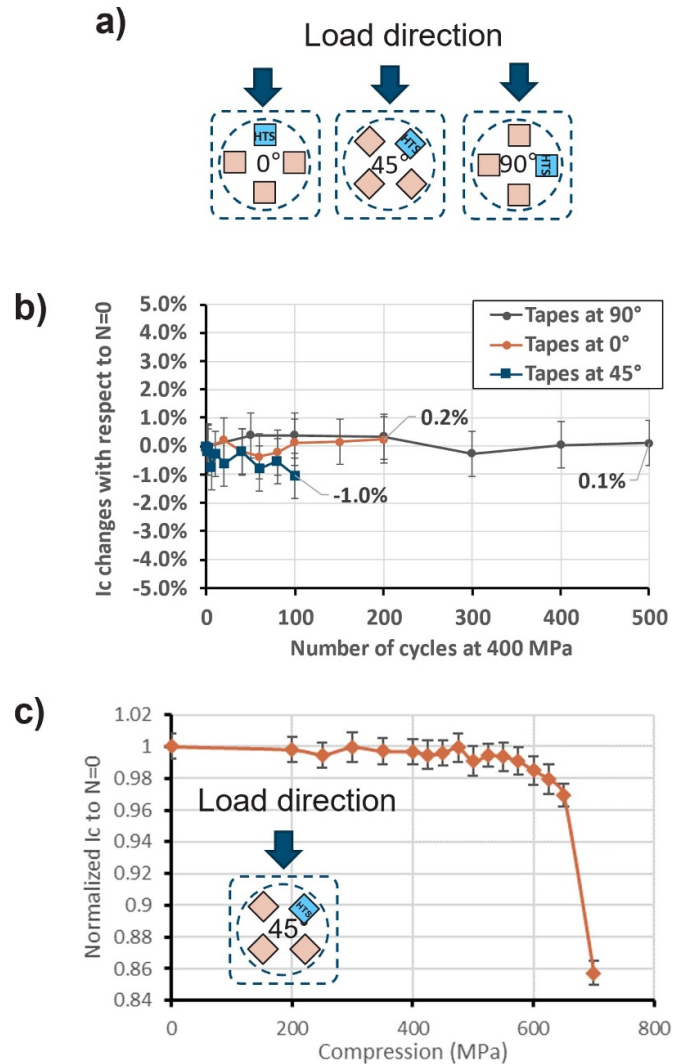


Figure 10. Transverse loading (a) orientations, (b) normalized (77 K, self-field) I_c evolution as a function of number of compressive cycles, N , for all orientations cycling from 200 MPa to 400 MPa for each cycle and unloading completely every few cycles for I_c measurements, and (c) after cycling at 400 MPa was complete, the 45° orientation sample I_c was measured after loading and unloading with increasing compression values up to 700 MPa. An irreversible limit is not observed below 600 MPa. All I_c measurements were done in the unloaded state.

experiments have been successfully carried out on arrays of insulated ITER conduits—loaded at cryogenic temperatures for tens of thousands of transverse compression cycles—with the breakdown voltage measured at room temperature after mechanical cycling (see [53, 54] for more details). The insulation chosen for PIT VIPER cables is modeled after ITER's glass-Kapton wrapped tapes as described in [55] with only slight modifications to reduce thickness. The same epoxy was used as in [55]. Three identical arrays of PIT VIPER cables were fabricated in a staggered pattern of alternating rows of four and five conductors with turn insulation around every conductor and two plies 0.2 mm-thick fiberglass between rows representing layer insulation (see figure 11). These samples

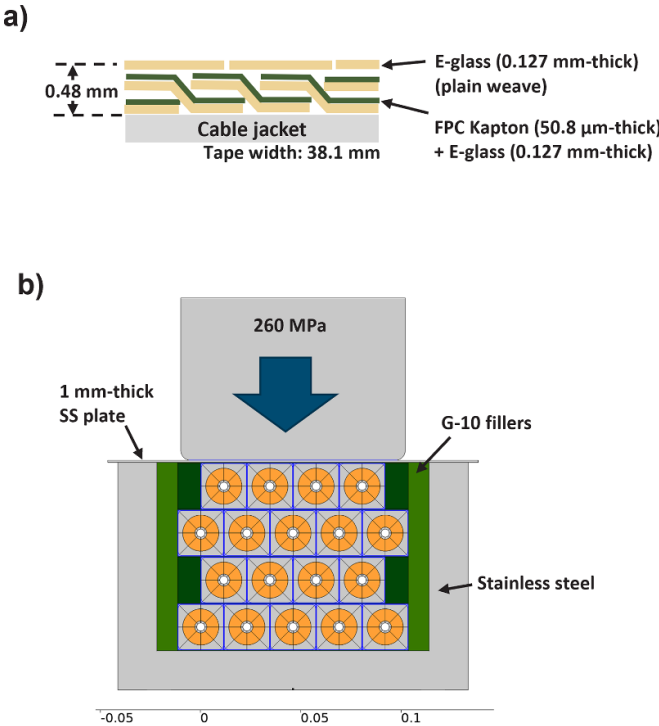


Figure 11. (a) A sketch of a cross section view (not to scale) along the length of the conductor showing the design of the turn insulation of SPARC CS and (b) configuration of the 4545 array test coupons.

were cycled for 70 000 cycles at 260 MPa and 77 K. The loading and the cycles were chosen for fatigue analysis using methods in [56], which suggests a conservative approach using more cycles, lower loading, and up to three samples for statistical purposes. The results are shown in figure 12 where a winding pack modulus of elasticity is approximated (after the first settling cycle) at ~ 75 GPa. This is a value that should be lower in real magnets, but is still much higher than that found in insulated arrays of non-soldered CICCs like ITER [53]. After 70 000 cycles at 260 MPa, all three samples were hi-pot tested and passed above 10 kV with leak currents under $0.05 \mu\text{A}$ and breakdown voltages above 13 kV except for an overloaded case discussed below. Values are shown in table 3. These breakdown values exceed the ‘ $2x + 1$ ’ criterion recommended by ITER [57] of two times the maximum operating voltage plus 1 kV, which for SPARC amounts to 1 kV and 3 kV for turn and layer insulation respectively.

Array 3 was further tested at 400 MPa for another 70 000 cycles. Photos of the samples after their compression cycles are shown in figure 13 as well as the stress-strain curves of the highly stressed sample showing significant plasticity and an elastic modulus drop from 66.0 GPa to 62.3 GPa (average measurement between 200 MPa and 300 MPa). This excessive deformation resulted in an electrical short on one of the top conductors (top left), with all other conductor pairs passing their respective 1 kV and 3 kV criterion with acceptable leak current values—albeit thirty times higher than those after 260 MPa.

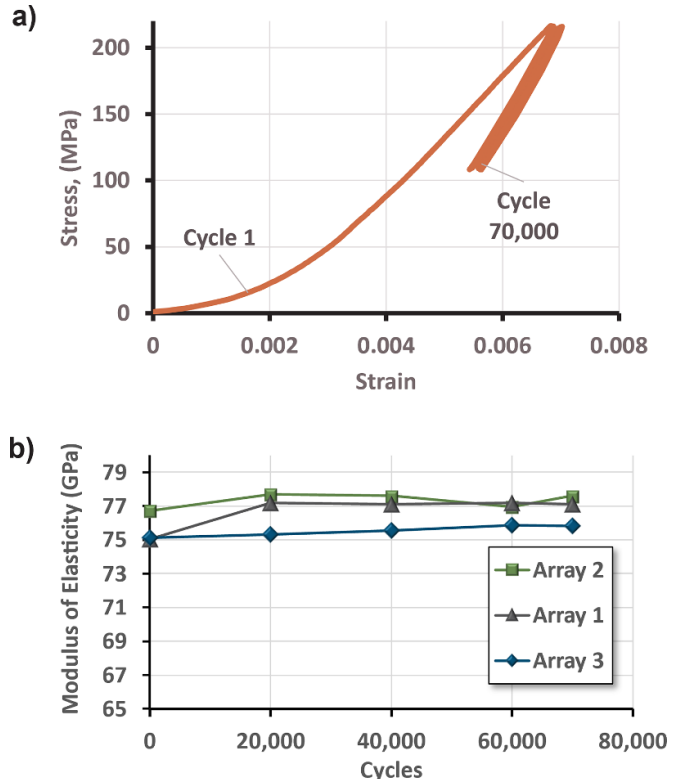


Figure 12. (a) Typical stress-strain curves of the units under test at 260 MPa (b) measured elastic modulus as a function of cycles.

This 400 MPa test was an attempt to understand edge cases observed in our latest models of SPARC CS. However, the level of plasticity obtained in pure transverse loading at 400 MPa is unlikely to be the same as in hoop loading of the same peak stress values. A follow-up experiment will be done with more accurate targets (below 400 MPa given that this target was a non-representative extreme) and including ground insulation with a geometry representative of the SPARC CS buffer region (i.e. the space between modules) to better understand this risk and its likelihood.

6. Risk 4: manufacturability

Between 2020 and 2023, CFS has fabricated several PIT VIPER samples of medium and long lengths to prove manufacturability at relevant scales. The samples and their risk-retirement purpose and outcomes are listed in table 4. Note that the first 100 m-long proof-of-concept sample had a significant underperformance, with an n -value below 10 and up to 23% lower I_c than predicted in some turns. An investigation revealed damage to the tapes during winding of this 100 m-long single layer. This has been alleviated since, with subsequent wound cable samples showing very good agreement with the theoretical I_c values and a very high n -value. The predicted cable I_c values shown in table 4 are calculated using the methods shown in appendices A and B.

Table 3. Leakage currents and breakdown voltages across neighboring conductors of the three identical arrays tested.

Array number	Target compression (MPa)	Highest leakage current reading at 3 kV (μ A)	Highest leakage current reading at 10 kV (μ A)	Average breakdown voltage (kV)	Lowest breakdown voltage (kV)
1	260	0.02	0.04	24.75	20
2	260	0.02	0.05	26.75	15
3	260	0.02	0.5	18.5	13
3	400	0.58 ^a	n/a	8.7 ^a	5.1 ^a

^a these values ignore the short observed at the top left conductor.

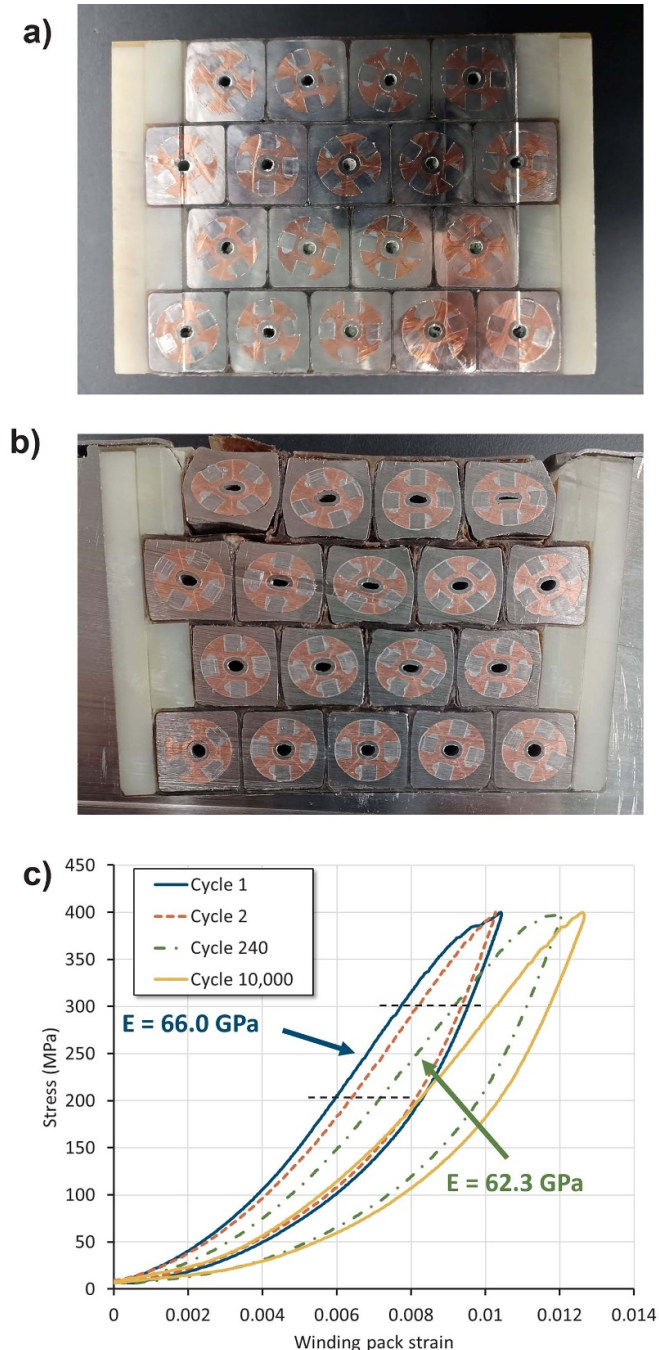


Figure 13. (a) Array 1 after 260 MPa for 70 000 cycles. (b) Array 3 after 260 MPa for 70 000 cycles and 400 MPa for 70 000 cycles where an electrical short on the top left conductor can be observed (c) stress-strain curves during compliance tests for array 3 loaded at 400 MPa. The deformation went beyond the capabilities of the instrumentation after 10 000 cycles and therefore is not plotted.

Table 4. PIT VIPER samples longer than two meters made to date.

Sample length (m)	Date of manufacture completion	Jacket geometry	# of HTS petals/total # of petals	Target self-field	Measured self-field		Measured n-value (77 K)	Purpose	Outcome
				77 K $I_c \pm 50$ (A)	77 K $I_c \pm 50$ (A)				
15	May 2021	Round	0/4	N/A	N/A	N/A	Proof of concept and hot-spot detection	Success	
3	September 2021	Round	1/4	4145	3720	22 ± 3	Stack IxB load qualification	Success	
3	September 2021	Round	4/4	6140	6450	18 ± 3	High current hot-spot detection	Success	
100	June 2022	Round	1/4	3540	2870	8 ± 1	Cable manufacturing qualification	Damage root cause identified	
38.7	October 2022	Square	4/4	4550	4330	23 ± 3	Cable manufacturing 2nd qualification. Quench studies, See section 8	Success	
40	February 2023	Square	4/4	9176	8754	29 ± 3	See section 9	Success	
39	April 2023	Square	4/4	9209	8592	27 ± 3	See section 9	Success	
43	March 2023	Square	4/4	9272	9049	33 ± 3	See section 9	Success	
45	April 2023	Square	4/4	9157	8617	31 ± 3	See section 9	Success	
3	March 2023	Square	4/4	28930	not measured	N/A	Joint resistance below 20 K	Success	
2.8	July 2023	Square	1/5	3230	3260	20.8 ± 3	Characterization of solder flowrates and times representative of PF4	Success	
59.5	September 2023	Square	0/5	N/A	N/A	N/A	PF style cable line qualification	Success	
58.5	September 2023	Square	0/5	N/A	N/A	N/A	PF style jacketing and winding qualification	Success	
58.5	October 2023	Square	4/5	2767	2743	21 ± 2.5	PF performance qualification	Success	
22	Exp. December 2023	Square	1/5	3287	TBD	TBD	PF-like solder flow qualification	TBD	

6.1. The solder process

As it has been discussed above, solder impregnation significantly improves the electromechanical properties of a superconducting cable. Soldered cable concepts have been proposed for fusion magnets in the past [58], however, this may not be recommended for AC magnets in ramped tokamaks made of low temperature superconductors (LTS) because the solder impregnation removes the intimate contact between the superconductor and the supercritical helium which is one of the main benefits of LTS CICC [59, 60]. The high temperature margin offered by HTS allows for solder use within the conductor, but the novelty of VIPER and PIT VIPER comes not only from the use of solder for reinforcement, but from the use of a vacuum-pressure impregnation (VPI) process which significantly improves the properties of the fill [61]. The details of this process are proprietary and therefore not disclosed in this manuscript.

The VPI process itself can lead to imperfect fill depending on the temperature profile and the flux used to remove oxides and wet the cable surfaces prior to the VPI. Figure 14 shows CT scans of a VIPER cable circa 2019 (top) and a PIT VIPER

cable circa 2022 (bottom) where the flux selection led to differences in the void fraction. Another important consideration for flux selection is the absence of halides, which are known to cause significant stress corrosion in austenitic stainless-steels over long periods of time [62, 63]—causing significant delays of major projects [64].

A significant concern regarding this process is temperature. Exposing REBCO to high temperatures can cause oxygen out-diffusion from grain boundaries, reducing its critical current [65–67]. The flow of solder past the tape also erodes the protective copper coating, which can expose the REBCO to further damage [68, 69]. Dedicated tests are being conducted to retire the risks of solder degradation, where solder flow comparable to the longest SPARC PF cables was optimized to produce minimal I_c degradation with encouraging results (see table 4). In addition, it should be noted that the cables used in IxB and compressive load tests (sections 4 and 5) were deliberately exposed to flow amounts and times prototypical of respective CS coils. This exposure is much longer than used for original VIPER SULTAN tests and addresses the risk that HTS tapes with coatings eroded by solder might have lower load tolerance.

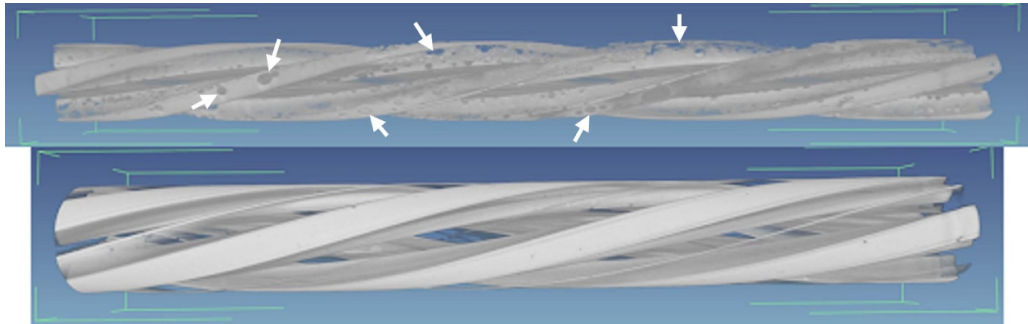


Figure 14. CT scan showing isolated solder where some porosity is observed and a few large voids are highlighted with white arrows. Top: a VIPER cable, circa 2019, using flux from manufacturer A. Bottom: a PIT VIPER cable, circa 2022, using flux manufacturer B.

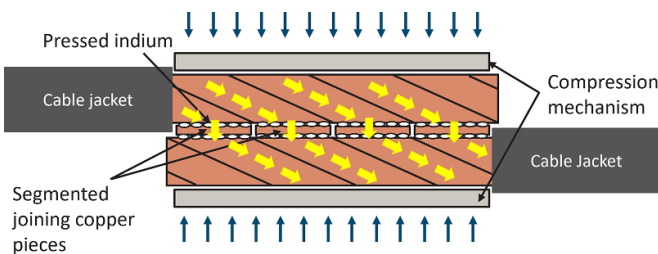


Figure 15. Basic concept of a PIT VIPER joint after the jacket is removed at the joint region. Wide solid arrows depict the current path; thin arrows show the compression.

7. Risk 5: joint performance

Due to the soldered nature of PIT VIPER cables, making a sintered joint similar to those developed for ITER [70] is not feasible. Even a butt joint [71] is challenging given that the cooling tube is trapped inside a monolithic conductor, and welding on its thin walls can easily develop helium leaks inside this heavily loaded winding pack. For this reason, our efforts have been focused solely on producing a PIT VIPER *lapped joint* based on the same concept as VIPER [13], with silver-plated surfaces and compressed indium wire—similar to some joints qualified for ITER in [72]. There are two competing design considerations related to cable joints in SPARC CS and PF magnets, (1) a resistance lower than $20\text{ n}\Omega$ to reduce ohmic heating and (2) a small footprint with segmented areas to reduce AC losses from changes in magnetic flux. To achieve this in a winding pack as compact as the SPARC CS, with the field direction perpendicular to the joint plane, it is necessary to break up the copper pieces joining the two lapped cables and to limit the contact areas to reduce large current loops within the joint. The basic concept of the PIT VIPER joint is shown in figure 15 where the yellow arrows show the main low-resistance path and therefore the discrete areas in which eddy currents could develop. To prepare these joints, the stainless-steel jacket of the fully-soldered cable must be removed in the jointing section of each cable, and the cable surfaces sanded to expose the copper former. Subsequent steps have been described elsewhere [13].

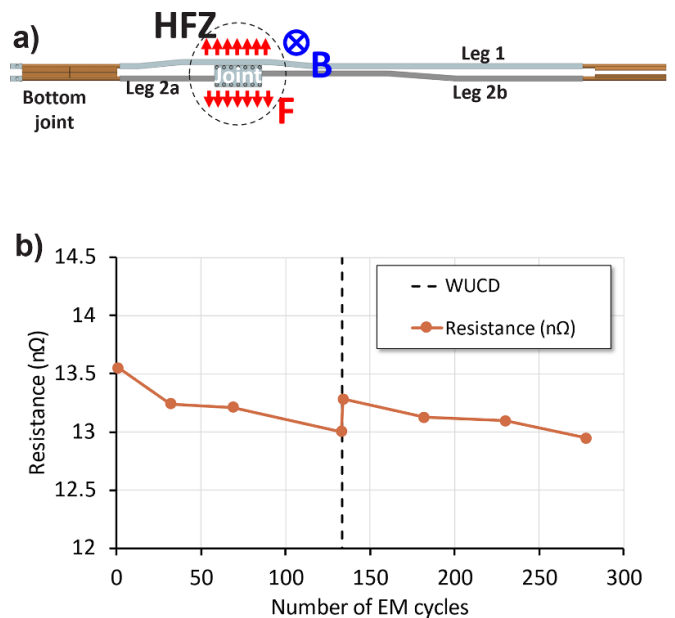


Figure 16. (a) SULTAN sample for PIT VIPER joint qualification (b) measured resistance of the lapped joint in the HFZ at 50 kA, 10.9 T and 15 K as a function of EM cycles cycles.

To study the feasibility and performance of these joints during and after EM cycling, three fully manufactured PIT VIPER cables were made to act as the two legs of a SULTAN sample (see figure 16). The setup consists of one three-meter-long section jointed at the bottom to one of two smaller sections having a lapped joint positioned to be aligned with the high-field zone (HFZ) of the SULTAN magnet as shown in figure 16(a). The bottom joint is outside of the scope of this experiment and therefore was made with a similar process to that described in [13]. The resistance evolution of this lapped PIT VIPER joint throughout an EM cycling campaign from zero to 80 kA at 10.9 T is shown in figure 16(b). The resistance values were measured between current pulses at a lower current (50 kA). Each 80 kA ramp represents an EM loading of 872 kN m^{-1} due to the background field of the SULTAN magnet. The setup and detailed results of this test will be presented in a separate publication [73].

8. Risk 6: QD

There are many sources of EM noise inside a tokamak. Not only are there various ramping magnets coupled to each other during a plasma run, but the plasma current itself and eddy currents generated in the various supporting structures can add to this high-noise environment. In LTS-based tokamaks, co-wound voltage taps [74] and other noise cancellation techniques such as central difference averaging [75] and magnet $i \cdot k$ (MIK) [76] have proven effective in their suppression of this EM noise with acceptable hold times [75, 77–79]. The challenge for HTS arises from the $10\times$ slower quench propagation velocity of REBCO [33] causing the quench zone to be orders of magnitude shorter than in LTS and therefore the voltage signal proportionately smaller. ITER conductors, for example, are estimated to require three to four meters of quenched length at 12 T, 40 kA, and 50 K for the voltage signal to rise above the threshold level of 250 mV with a signal-to-noise ratio (SNR) of 10 [77, 80], that is roughly $20\text{ n}\Omega\text{ cm}^{-1}$. PIT VIPER is estimated to have roughly $0.5\text{ n}\Omega\text{ cm}^{-1}$ under similar conditions, which makes it unrealistic to detect voltages in the level a few tens of millivolts using voltage tap-based approaches in SPARC. Therefore, the chosen QD technology for PIT VIPER and SPARC is based on fiber bragg grating (FBG), which, despite its relative immaturity as a QD method, has the significant advantage of being immune to EM noise.

In the past, we have developed experimental approaches [81] that forgo the spatial resolution of discrete FBG peaks and instead use a much higher density array producing a complex spectrum. The detection mechanism, therefore, focuses on identifying changes in the spectrum, instead of tracking individual peak shifts as is often the case for FBG-based strain sensors [82, 83]. The resulting figure of merit is produced by signal-processing algorithms as a single, unitless value which increases when changes in the fiber spectra are observed. This is referred to as our algorithm response or the ‘quench signal’. To explore the signal shape and develop the algorithm responses for a fully manufactured PIT VIPER cable, a 15-meter-long test cable (see table 4) was made and instrumented. Through this sample, improvements on the fiber location and FBG wavelength and spacing were made—compared to that used on the early VIPER prototypes [81]. The sample was instrumented with one fiber per stack, with each fiber having 300 evenly distributed FBGs with wavelengths between 1510 and 1590 nm. Further details on fiber configuration are proprietary technology. This cable was tested in liquid nitrogen and equipped with heaters at random locations along the length as a proof-of-principle method despite not having any current or HTS. The spectrum signal during firing of the heaters and their processed values are shown in figure 17, where the processed signal matches the temperature rise with very good SNR.

A much more rigorous and complex follow-up experiment used a 38.7 m-long PIT VIPER cable tested at SPARC-relevant current and temperatures. This 10-turn coil was heavily instrumented—with more than 70 co-wound voltage taps, more than 10 heaters, and up to 25 cernox temperature sensors—to understand quench dynamics and fiber optic responses on fully-developed quench events and to fine-tune

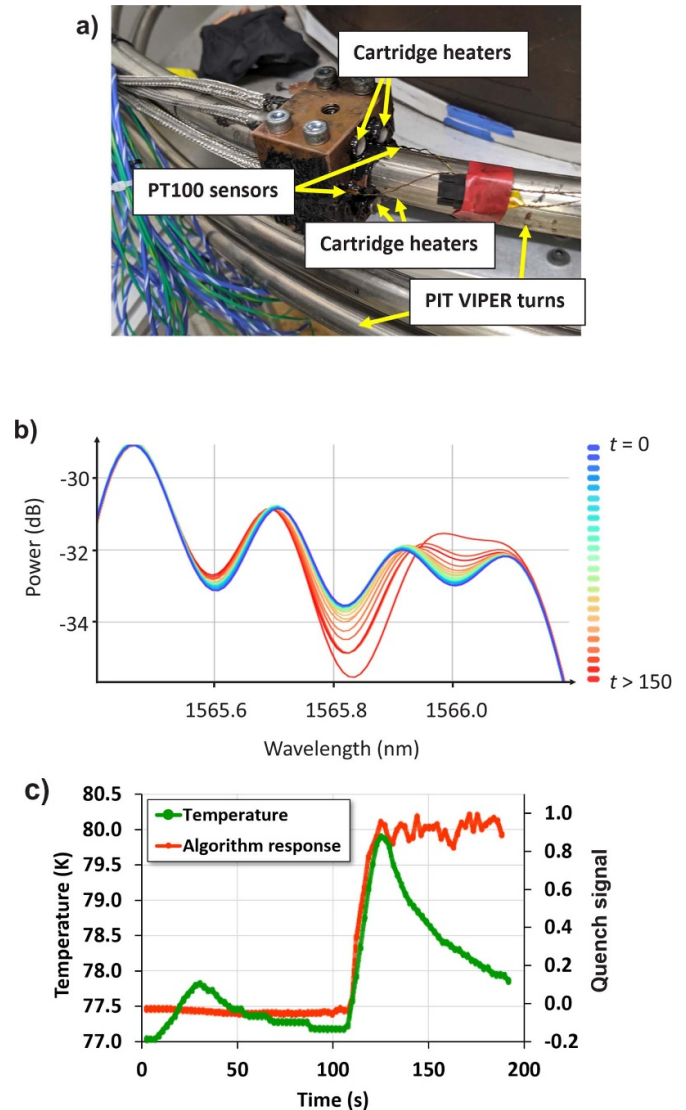


Figure 17. (a) Photo of the cartridge heaters and copper heating block on a 15 meter-long PIT VIPER cable. (b) FBG spectral shape changes observed in PIT VIPER cables tested in LN₂ with heaters attached. (c) The quench detection algorithm responses during heater triggers.

the algorithm responses for these operating currents and temperatures. This cable underwent 70 quench events (with currents ranging between 28 and 43 kA and temperatures between 23 K and 30 K) in which the FBG fibers produced an EM immune signal with very high SNR. The quenches were induced using surface heaters on the cable. A voltage bridge circuit across the coil was used as the primary QD method. For each quench, the fiber optic signals were captured, post-processed, and compared to the signal from arrays of voltage-taps (spaced by $\sim 5\text{ cm}$) near the quench zone. A few examples of these quench events and their algorithm responses are found in figure 18, where voltage traces (captured by voltage tap pairs close to the quench region) and the spectral change signal (i.e. ‘quench signal’) respond similarly to the thermal runaway triggered by a heater pulse at $t = 0$ lasting a few seconds. The voltage increase from the quench events were closely matched

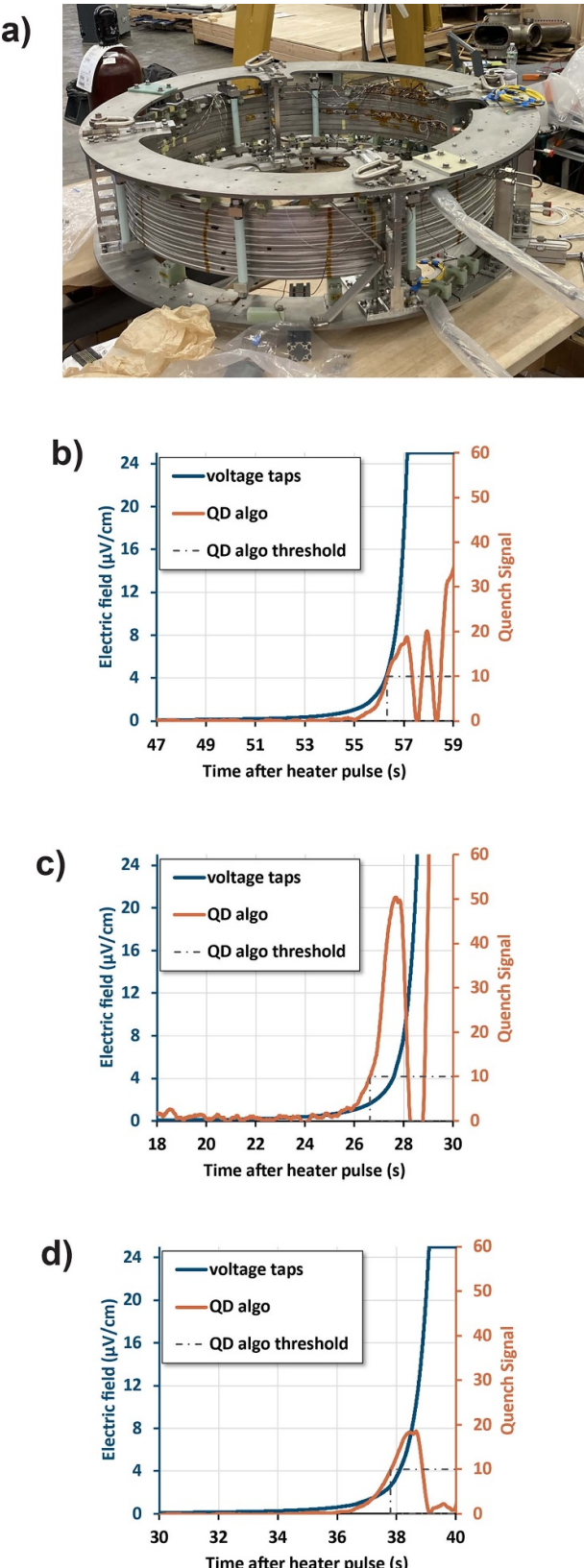


Figure 18. (a) A 38.7 m-long PIT VIPER cable instrumented and designed to understand quench dynamics and fiber optic responses on fully-developed quench events. (b)–(d) the spectral change and the voltage measured in the quench region for quenches at 37.4 kA, 35.7 kA, and 33.9 kA respectively. Voltage tap measurement is limited to 0.5 mV by the DAQ.

Table 5. The SPARC central solenoid model coil operational parameters.

Parameter	Value
Inner radius	0.602 m
Outer radius	0.708 m
Height	0.348 m
Number of turns per layer	10
Number of layers	4
Petals per cable	4
Fibers per cable	4
HTS count per cable	136
Cable former diameter	18 mm
Jacket side dimension	23 mm
Turn insulation thickness	0.5 mm
Layer insulation thickness	0.4 mm
Operational temperature	18–25 K
Peak field	5.7 T
Peak ramp rate (at discharge)	$\sim -4 \text{ T s}^{-1}$
Peak ramp rate (linear)	0.37 T s^{-1}
Inductance	2.982 mH
I_{op}/I_c at 50 kA (designed)	0.85
Stored magnetic energy	3.728 MJ

by the fiber response in all 70 quenches. It is important to highlight that for all quenches (except for the last one), there were no detectable changes in I_c during operation and the I_c values measured had similar percentage deviation from predictions as observed during our 77 K testing, see table 4. The last quench was catastrophic and was a result of operator error (the wrong setting was chosen for the QD voltage threshold). The details of the test campaign of this 38.7 m-long PIT VIPER layer and all its quench events are still being analyzed and will be part of a future publication.

9. Risk 7: integration and testing

The fabrication of the SPARC CSMC encompasses a variety of risks inherent to any first-of-a-kind magnet fabrication and operation, such as cable damage during integration, insulation defects, and/or operational issues. The operational parameters of this coil are shown in table 5. Its peak field (5.7 T), despite being lower than SPARC CS and PF, still matches their current and temperature (which are the main sources of variability in quench dynamics). As noted in table 5, the linear field ramp rates are limited to 0.37 T s^{-1} ; this comes from limitations of the test facility, which was designed for the SPARC TFMC (a no-insulation magnet) [15]. However, using fast discharges within the facility limitations, dB/dt values starting at -4 T s^{-1} can be obtained with a decay constant of 1.4 s. Additionally, the facility has been equipped with fiber optic feedthroughs and cables which were already tested for the test coil shown in section 8. The operational stresses and strains are shown in figure 19.

Despite the low operational voltages, the insulation in CSMC is rated for SPARC CS operation which can be as high as 10 kV to ground, 3 kV layer-to-layer, and 1 kV

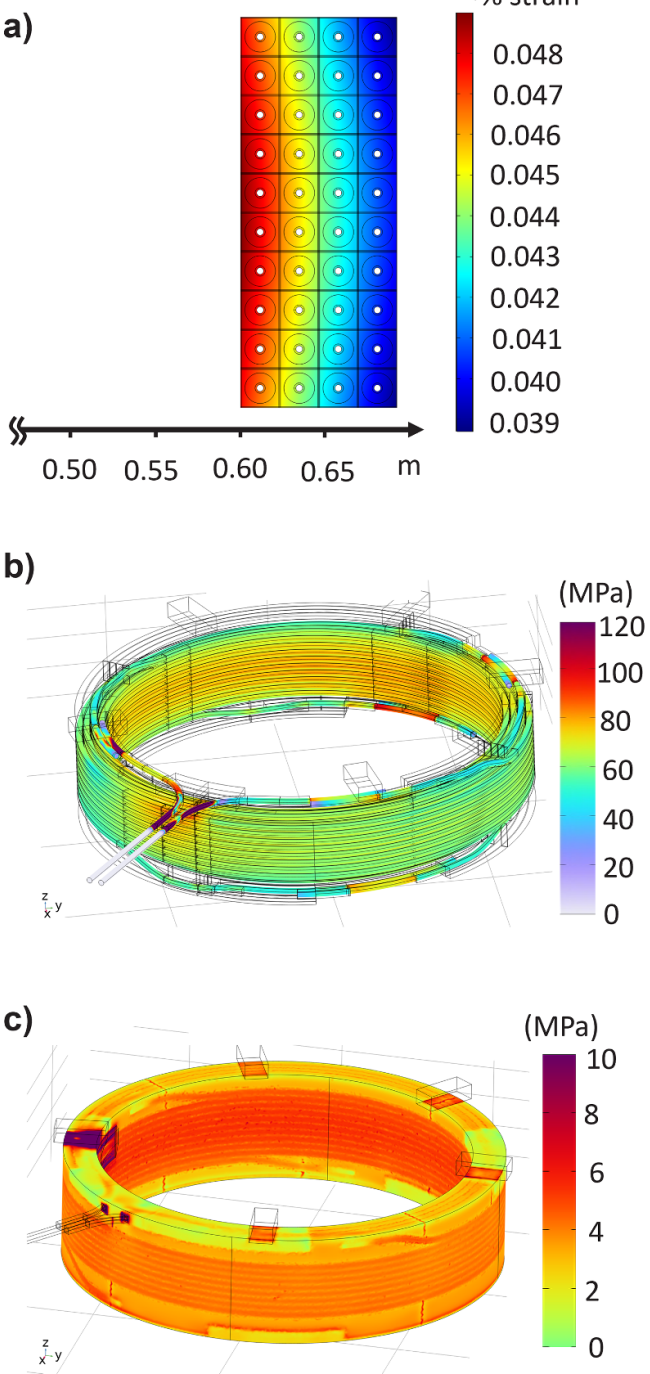


Figure 19. The SPARC central solenoid model coil (CSMC) design. (a) 2D model of the epoxied winding pack hoop strain during peak field. (b) von mises stresses of the CSMC on the conductor jacket (not showing the stresses on the insulation). (c) von-mises stresses of the CSMC on the ground insulation.

turn-to-turn. The ground insulation is composed of six layers glass-kapton-glass tape poloidally wrapped around the coil with 50% overlap. Furthermore, CSMC uses ground insulation ‘feedthroughs’ for cooling tubes and fiber optics developed and tested at CFS to up to 21 kV in Paschen conditions [84]. These components and their electrical isolation are an important focus for this coil fabrication and subsequent SPARC coils,

Table 6. The SPARC central solenoid model coil test objectives.

Category	Test objectives during CSMC test campaign
Cable performance	Operate CSMC at 50 kA and 20 K without generating a quench.
Cable performance	Obtain an I_c (T) curve between 25 K and 45 K to compare with modeled predictions.
Cable performance	Measure joint resistances.
Cable performance	Measure the magnet AC losses ramps via calorimetry during fast discharges ($\sim 4 \text{ T s}^{-1}$) and linear ramps ($\sim 0.1 \text{ T s}^{-1}$).
Magnet-related	Subject the insulation to at least two thermal cycles for a future room temp paschen test.
Magnet-related	Measure the magnet’s radial and axial modulus (as measured over the ground insulation).
Fiber spectra	Obtain fiber cooldown data to confirm models and understand any other sources of attenuation.
Fiber spectra	Prediction of spectral changes after cooldown and at specific current (magnet strain) values.
Fiber spectra	Measure the fiber spectra during steady state to understand FBG drift due to joint heating.
Fiber spectra	Capture fiber spectra during high strain events.

given the high risk associated with paschen failures during magnet commissioning and operation [84–86]. This coil was tested in August 2024 as a stand-alone coil at the MIT test facility [87] with flowing helium gas at 20 K or higher, and currents up to 50 kA. The test objectives are outlined in table 6 and the test results will be published in a separate publication.

10. Conclusions

A novel superconducting cable technology based on REBCO tape-stacks has been developed for pulsed magnets in compact tokamaks operating up to 25 T at 20 K and having an engineering critical current density in the range of $\sim 100 \text{ A mm}^{-2}$. This CICC, called PIT VIPER, is composed of twisted copper former ‘petals’ with stacks of ~ 90 REBCO tapes each. Electrical insulation is applied between petals and a seamless tube through the middle for gaseous helium coolant. The conduit is a seam-welded, high-strength austenitic stainless-steel jacket that also serves as the vessel for a fabrication step involving molten solder VPI of the cable—turning it into a monolithic conductor. This cable technology can sustain up to 600 MPa of transverse compression when applied to a single cable without degradation of current transport properties (tested in liquid nitrogen). Similarly, negligible I_c degradation or T_{cs} changes were observed with up to 300 kN m^{-1} of $I \times B$ loading per stack (tested at the SULTAN magnet facility). Additionally, the lack of empty space within the conduit, with no incompressible media (except inside the cooling tube), gives this CICC an exceptional winding-pack modulus ($\sim 70 \text{ GPa}$) which prevents high strain on the insulation upon loading and preserves electrical integrity. The key

feature of this novel technology are the segmented copper petals, which reduce AC losses up to 15 times lower than its predecessor technology and enables the operation of high-field, pulsed, compact tokamaks like SPARC and the ARC fusion pilot plant. To maintain the low AC-loss properties in PIT VIPER-based magnets, joint length and surface contact between cables is limited to avoid large current loops within the joint. Nonetheless, a robust joint mechanism has been developed which can have joint resistances in the range of $15 \text{ n}\Omega$ with excellent EM loading resilience. Finally, the fiber optic-based QD system shows encouraging results at relevant operational currents and temperatures. As part of the risk-retirement campaign, a model coil operating at 50 kA with a peak field of 5.7 T and a ramp rate discharge starting at -4 T s^{-1} was tested in August 2024—as a comprehensive technology-readiness test in preparation for the CS and PF coil fabrication for SPARC.

This new cable technology was designed for mass production and is not limited to tokamak use. Its mechanical stability, high current density, and fast-ramping capabilities make it suitable for high ramping field experiments or test-beds where bore sizes above $\sim 200 \text{ mm}$ and high current densities are desired. An accumulated total of more than 500 m of PIT VIPER have been made to date with excellent quality and reproducibility, proving not only the performance of this new technology but also the manufacturing capabilities and supply-chain needs for the volumes and scales required for both SPARC (a demonstration device) and ARC (a fusion power plant).

Data availability statement

The data cannot be made publicly available upon publication because they contain commercially sensitive information. The data that support the findings of this study are available upon reasonable request from the authors.

Acknowledgment

This work was funded by ARPA-E Award Number DE-AR0001259 and by Commonwealth Fusion Systems. The authors would like to thank Peter Titus and Tom Painter for attending design reviews and providing useful advice, as well as Dash Weeks, Ross Rentz, and Jake Benzing at NIST for mechanical testing support.

Appendix A. Cable I_c predictions

The predicted cable I_c values shown in table 4 are calculated by scaling the I_c (77 K, SF) of each of the tapes in the cable to the manufacturer-specific data sets, in the J_e (B, T, θ) space. See appendix B for further details on tape datasets. The scaling provides a tape J_c (B, T, θ) for each of the tapes in the cable which is then weighed based on the number of tapes, their thickness, and the length of tape to get the stack I_c (B, T, θ). This stack I_c is fed to a model of the PIT VIPER cable using

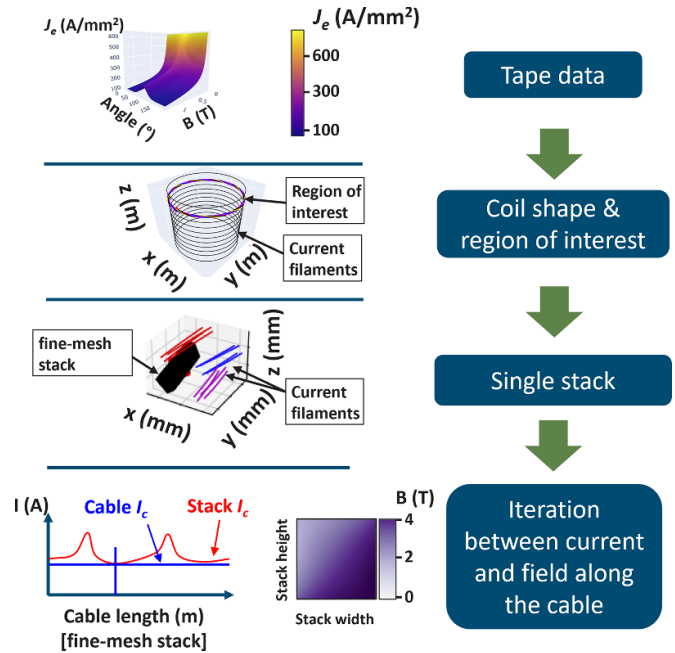


Figure 20. Hierarchical filamentization and process steps for predicting cable I_c . Software developed by Robert Granetz (MIT) and James Logan (CFS).

a hierarchical filamentization method developed in [88]. At the highest level, the cable/magnet is represented by a single line of current at the cable's axis obeying the Biot–savart law to obtain the field gradient at the macro scale. Then, at the meso scale (several cable twist pitches), the HTS tape stacks are represented by a few lines of current also obeying Biot–savart and following the stack's axis. The stacks are assumed to be insulated from one another. At the micro level, for the length of one or two twist pitches, one of the HTS tape stacks is represented by a mesh of dozens of filaments limited by the stack I_c (B, T, θ). Using this hierarchy of currents, a magnetic field is quickly solved for a given current. This field is then compared to the stack I_c (B, T, θ) curves and is increased iteratively until the lowest point in the B, T, θ space of the fine mesh reaches I_c . This current value is chosen as the cable I_c . This process is illustrated in figure 20.

Appendix B. Tape datasets

The manufacturer-specific data sets were built by averaging and symmetrizing high-fidelity I_c (B, T, θ) measurements on dozens of reels from the same manufacturer. The I_c (77 K, SF) of each of the reels in a cable are taken on full-width tapes with 10 mm voltage tap separation, and low-temperature angular measurements were taken on 0.4 mm wide bridged samples with 5 mm voltage tap separation on a Supercurrent measurement system manufactured by HTS-110 and Robinson Research Institute [89]. I_c of these single tapes was defined at an electric field criterion of $1 \mu\text{V cm}^{-1}$. The data processing includes a symmetrization step which averages the measured data points equidistant from 90° , which is defined where $B \parallel$ tape-plane, and applied to both sides [90].

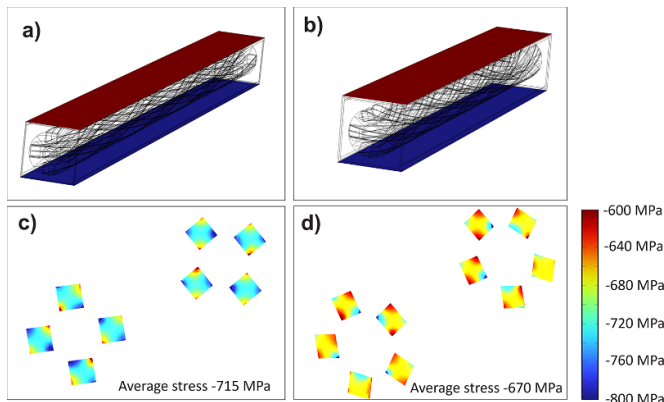


Figure 21. Multiphysics models of a (a) four-petal cable and a (b) five-petal cable subjected to external strains of -0.6% longitudinally and -0.4% transversely. The stresses in the HTS of (c) the four-petal cable and a (d) the five-petal cable show similar magnitude at the extremes and average values that vary only by 7%.

Appendix C. PIT VIPER mechanical models

Due to the monolithic nature of PIT VIPER, it was initially assumed that the number of petals plays a minor role in the strains observed in the REBCO tapes—i.e. each petal is mechanically independent, and forces are kept within it. This assumption has proven reliable under single-stack IxB loading at SULTAN (as shown in sections 4 and 7 as well as experiments on VIPER conductors [13]). Multiphysics models were validated through these experiments, and these models were further expanded to external loads such as those observed in SPARC CS. Figure 21 shows Multiphysics models of a five-petal and a four-petal cable subjected to external strains of -0.6% longitudinally and -0.4% transversely, with the third axis (side faces) unbound. The results show stresses generated in the HTS of similar magnitude and distribution, with an average difference of only 7%. This is largely owed to the monolithic nature of PIT VIPER provided by the solder VPI process supported by the copper former and the stainless steel jacket. Other experiments have shown that even jacket yielding still does not seem to irreversibly affect the HTS performance in the conductor [45].

ORCID iDs

Charlie Sanabria [ID](https://orcid.org/0000-0001-5017-5309) <https://orcid.org/0000-0001-5017-5309>
 Alexey Radovinsky [ID](https://orcid.org/0000-0002-0053-2467) <https://orcid.org/0000-0002-0053-2467>
 Kiran Uppalapati [ID](https://orcid.org/0000-0002-1690-0586) <https://orcid.org/0000-0002-1690-0586>
 Elle Allen [ID](https://orcid.org/0009-0004-3352-2275) <https://orcid.org/0009-0004-3352-2275>
 David Chavarria [ID](https://orcid.org/0009-0001-3158-9909) <https://orcid.org/0009-0001-3158-9909>
 Kristen Metcalfe [ID](https://orcid.org/0009-0007-4223-5149) <https://orcid.org/0009-0007-4223-5149>
 Amanda Hubbard [ID](https://orcid.org/0000-0001-8469-780X) <https://orcid.org/0000-0001-8469-780X>
 Amy Watterson [ID](https://orcid.org/0000-0002-7857-3701) <https://orcid.org/0000-0002-7857-3701>
 Benjamin Weinreb [ID](https://orcid.org/0000-0003-2302-9167) <https://orcid.org/0000-0003-2302-9167>
 Elizabeth Brownell [ID](https://orcid.org/0000-0002-1236-4835) <https://orcid.org/0000-0002-1236-4835>

- Erica Salazar [ID](https://orcid.org/0000-0003-3011-9013) <https://orcid.org/0000-0003-3011-9013>
 Owen Duke [ID](https://orcid.org/0009-0003-5127-2874) <https://orcid.org/0009-0003-5127-2874>
 Matt Hicks [ID](https://orcid.org/0009-0003-6522-9172) <https://orcid.org/0009-0003-6522-9172>
 Ashleigh Francis [ID](https://orcid.org/0000-0001-9165-0209) <https://orcid.org/0000-0001-9165-0209>
 JL Cheng [ID](https://orcid.org/0000-0002-6607-6134) <https://orcid.org/0000-0002-6607-6134>
 Aliya Greenberg [ID](https://orcid.org/0009-0004-9206-2619) <https://orcid.org/0009-0004-9206-2619>
 Vinny Fry [ID](https://orcid.org/0000-0002-1110-0563) <https://orcid.org/0000-0002-1110-0563>
 Ronak Padukone [ID](https://orcid.org/0009-0009-6791-0918) <https://orcid.org/0009-0009-6791-0918>
 Theodore Golfinopoulos [ID](https://orcid.org/0000-0002-0898-5217) <https://orcid.org/0000-0002-0898-5217>
 Philip C Michael [ID](https://orcid.org/0000-0003-4906-6169) <https://orcid.org/0000-0003-4906-6169>
 Rodney Badcock [ID](https://orcid.org/0000-0003-0219-9570) <https://orcid.org/0000-0003-0219-9570>
 Mike Davies [ID](https://orcid.org/0000-0003-4841-5830) <https://orcid.org/0000-0003-4841-5830>
 Arvid Hunze [ID](https://orcid.org/0000-0002-9060-2894) <https://orcid.org/0000-0002-9060-2894>
 Bart Ludbrook [ID](https://orcid.org/0000-0001-9955-1715) <https://orcid.org/0000-0001-9955-1715>
 Ramesh Gupta [ID](https://orcid.org/0000-0002-9450-7341) <https://orcid.org/0000-0002-9450-7341>
 Hugo Bajas [ID](https://orcid.org/0000-0003-4871-4750) <https://orcid.org/0000-0003-4871-4750>
 Christoph Mueller [ID](https://orcid.org/0009-0004-8159-699X) <https://orcid.org/0009-0004-8159-699X>
 Kamil Sedlak [ID](https://orcid.org/0000-0002-2090-1709) <https://orcid.org/0000-0002-2090-1709>
 Brandon Sorbom [ID](https://orcid.org/0000-0002-2110-6766) <https://orcid.org/0000-0002-2110-6766>
 Daniel Brunner [ID](https://orcid.org/0000-0002-8753-1124) <https://orcid.org/0000-0002-8753-1124>

References

- [1] Creely A 2020 Overview of the SPARC tokamak *J. Plasma Phys.* **86** 865860502
- [2] Usozkin A, Freyhardt H C, Issaev A, Dzick J, Knoke J, Oomen M P, Leghissa M and Neumueller H-W 2003 Large area YBCO-coated stainless steel tapes with high critical currents *IEEE Trans. Appl. Supercond.* **13** 2452–7
- [3] Watanabe T, Kuriki R, Iwai H, Muroga T, Miyata S, Ibi A, Yamada Y and Shiohara Y 2005 High rate deposition by PLD of YBCO films for coated conductors *IEEE Trans. Appl. Supercond.* **15** 2566–9
- [4] Selvamanickam V, Chen Y, Xiong X, Xie Y, Zhang X, Qiao Y, Reeves J, Rar A, Schmidt R and Leneseth K 2007 Progress in scale-up of second-generation HTS conductor *Physica C* **463–465** 482–7
- [5] Majkic G, Galstyan E and Selvamanickam V 2015 High performance 2G-HTS wire using a novel MOCVD system *IEEE Trans. Appl. Supercond.* **25** 1–4
- [6] Molodyk A *et al* 2021 Development and large volume production of extremely high current density YBa₂Cu₃O₇ superconducting wires for fusion *Sci. Rep.* **11** 1
- [7] Tsuchiya K, Wang X, Fujita S, Ichinose A, Yamada K, Terashima A and Kikuchi A 2021 Superconducting properties of commercial REBCO-coated conductors with artificial pinning centers *Supercond. Sci. Technol.* **34** 105005
- [8] Paidpillai M *et al* 2023 Development of 50-Meter RE-Ba-Cu-O tapes with critical current over 1750 A/12mm at 65 K, 0.25 T by advanced-MOCVD *IEEE Trans. Appl. Supercond.* **33** 1–5
- [9] Prabhakar A 2023 DOE announces \$46 million for commercial fusion energy development *Energy.gov*. (available at: www.energy.gov/articles/doe-announces-46-million-commercial-fusion-energy-development) (Accessed 9 September 2023)
- [10] Jennifer G 2023 Fact sheet: developing a bold vision for commercial fusion energy | OSTP *The White House* (available at: www.whitehouse.gov/ostp/news-updates/2022/03/15/fact-sheet-developing-a-bold-vision-for-commercial-fusion-energy/) (Accessed 9 September 2023)

- [11] Freeman G 2023 Towards fusion energy: proposals for a regulatory framework GOV.UK (available at: www.gov.uk/government/consultations/towards-fusion-energy-proposals-for-a-regulatory-framework) (Accessed 9 September 2023)
- [12] Sorbom B N *et al* 2015 ARC: a compact, high-field, fusion nuclear science facility and demonstration power plant with demountable magnets *Fusion Eng. Des.* **100** 378–405
- [13] Hartwig Z S *et al* 2020 VIPER: an industrially scalable high-current high-temperature superconductor cable *Supercond. Sci. Technol.* **33** 11LT01
- [14] Takayasu M, Chiesa L, Allen N C and Minervini J V 2016 Present status and recent developments of the twisted stacked-tape cable conductor *IEEE Trans. Appl. Supercond.* **26** 25–34
- [15] Hartwig Z S *et al* 2024 The SPARC toroidal field model coil program *IEEE Trans. Appl. Supercond.* **34** 1–16
- [16] Whyte D G *et al* 2024 Experimental assessment and model validation of the SPARC toroidal field model coil *IEEE Trans. Appl. Supercond.* **34** 1–18
- [17] Vieira R F *et al* 2024 Design, fabrication, and assembly of the SPARC toroidal field model coil *IEEE Trans. Appl. Supercond.* **34** 1–16
- [18] Riva N *et al* 2023 Development of the first non-planar REBCO stellarator coil using VIPER cable *Supercond. Sci. Technol.* **36** 105001
- [19] Campbell A M 1982 A general treatment of losses in multifilamentary superconductors *Cryogenics* **22** 3–16
- [20] Kar S, Sandra J S, Luo W, Kochat M, Jaroszynski J, Abraimov D, Majkic G and Selvamanickam V 2019 Next-generation highly flexible round REBCO STAR wires with over 580 A mm⁻² at 4.2 K, 20 T for future compact magnets *Supercond. Sci. Technol.* **32** 10LT01
- [21] Goldacker W, Grilli F, Pardo E, Kario A, Schlachter S I and Vojenčíak M 2014 Roebel cables from REBCO coated conductors: a one-century-old concept for the superconductivity of the future *Supercond. Sci. Technol.* **27** 093001
- [22] Solovyov V and Farrell P 2016 Exfoliated YBCO filaments for second-generation superconducting cable *Supercond. Sci. Technol.* **30** 014006
- [23] Uglietti D, Kang R, Wesche R and Grilli F 2020 Non-twisted stacks of coated conductors for magnets: analysis of inductance and AC losses *Cryogenics* **110** 103118
- [24] Bykovsky N, Uglietti D, Wesche R and Bruzzone P 2018 AC loss in HTS fusion cables: measurements, modeling, and scaling laws *IEEE Trans. Appl. Supercond.* **28** 1–5
- [25] Radovinsky A, Sanabria C, Craighill C, Uppalapati K, Creely A and Brunner D Partitioned superconducting cable (available at: <https://patentscope.wipo.int/search/en/detail.jsf?docId=WO2021178697>) (Accessed 10 September 2021–4 October 2022)
- [26] Muzzi L *et al* 2023 Design and feasibility assessment of an HTS sector shaped high-current conductor for fusion coils *IEEE Trans. Appl. Supercond.* **33** 1–6
- [27] Grilli F, Pardo E, Stenvall A, Nguyen D N, Yuan W and Gömöry F 2014 Computation of losses in HTS under the action of varying magnetic fields and currents *IEEE Trans. Appl. Supercond.* **24** 78–110
- [28] Takayasu M, Chiesa L, Noyes P D and Minervini J V 2017 Investigation of HTS twisted stacked-tape cable (TSTC) conductor for high-field, high-current fusion magnets *IEEE Trans. Appl. Supercond.* **27** 1–5
- [29] van der Laan D, Weiss J D and McRae D M 2019 Status of CORC® cables and wires for use in high-field magnets and power systems a decade after their introduction *Supercond. Sci. Technol.* **32** 033001
- [30] Talantsev E F, Badcock R A, Mataira R, Chong S V, Bouloukakis K, Hamilton K and Long N J 2017 Critical current retention of potted and unpotted REBCO Roebel cables under transverse pressure and thermal cycling *Supercond. Sci. Technol.* **30** 045014
- [31] McIntyre P M, Rogers J and Sattarov A 2021 Blocks-in-conduit: REBCO cable for a 20T@20K toroid for compact fusion tokamaks *IEEE Trans. Appl. Supercond.* **31** 1–5
- [32] Sytnikov V and Lelekhov S 2021 New HTS conductor design for large scale applications *IEEE Trans. Appl. Supercond.* **31** 1–5
- [33] van Nugteren J, Dhalle M, Wessel S, Krooshoop E, Nijhuis A and ten Kate H 2015 Measurement and analysis of normal zone propagation in a ReBCO coated conductor at temperatures below 50K *Phys. Proc.* **67** 945–51
- [34] Baldzuhn J *et al* 2019 Spark detection and search for high-voltage paschen leaks in a large superconducting coil system *IEEE Trans. Plasma Sci.* **47** 5125–38
- [35] Ulbricht A *et al* 2005 The ITER toroidal field model coil project *Fusion Eng. Des.* **73** 189–327
- [36] Aviles Santillana I, Sgobba S, Castillo Rivero S, Libeyre P, Jong C and Everitt D 2019 Post-mortem analysis of ITER CS helium inlets fatigue tested at cryogenic temperature *Fusion Eng. Des.* **146** 642–6
- [37] Gaio E, Maistrello A, Novello L, Matsukawa M, Perna M, Ferro A, Yamauchi K and Piovani R 2018 The new technological solution for the JT-60SA quench protection circuits *Nucl. Fusion* **58** 075001
- [38] Rossi L 2007 The large hadron collider and the role of superconductivity in one of the largest scientific enterprises *IEEE Trans. Appl. Supercond.* **17** 1005–14
- [39] Gupta R *et al* 2016 Design, construction, and testing of a large-aperture high-field HTS SMES coil *IEEE Trans. Appl. Supercond.* **26** 1–8
- [40] Sedlak K, Bruzzone P, Sarasola X, Stepanov B and Wesche R 2017 Design and R&D for the DEMO toroidal field coils based on Nb3Sn react and wind method *IEEE Trans. Appl. Supercond.* **27** 1–5
- [41] Kwasnitza K 1977 Scaling law for the ac losses of multifilament superconductors *Cryogenics* **17** 616–20
- [42] Bruzzone P, Anghel A, Fuchs A, Pasztor G, Stepanov B, Vogel M and Vecsey G 2002 Upgrade of operating range for SULTAN test facility *IEEE Trans. Appl. Supercond.* **12** 520–3
- [43] Gupta R 2019 Common-coil Nb3Sn dipole program at BNL *Nb3Sn Accelerator Magnets: Designs, Technologies and Performance Particle Acceleration and Detection* ed D Schoerling and A V Zlobin (Springer) pp 371–94
- [44] Takayasu M, Chiesa L, Bromberg L and Minervini J V 2011 HTS twisted stacked-tape cable conductor *Supercond. Sci. Technol.* **25** 014011
- [45] Diaz-Pacheco R Electromechanical properties of SPARC CS and PF superconductor cables under relevant transverse and axial compression *11th Workshop on Mechanical and Electromagnetic Properties of Composite Superconductors* (Spokane, Washington, USA, 14 June 2024) (available at: <https://nationalmaglab.org/news-events/events/for-scientists/mechanical-and-electromagnetic-properties-of-composite-superconductor-workshop/>)
- [46] Bruzzone P *et al* 2010 Status report of the SULTAN test facility *IEEE Trans. Appl. Supercond.* **20** 455–7
- [47] Joshi S, Cozzolino J, Gupta R and Sampson W 2020 Measurements of the effects of compressive loading on the narrow side of the HTS TAPE *IEEE Trans. Appl. Supercond.* **30** 1–5
- [48] Yan J, Wang K, Gao Y, Zhou Y and Nijhuis A 2022 Investigating the effect of transverse compressive loads on

- the electromagnetic performance of superconducting CORC® cables *Supercond. Sci. Technol.* **35** 115006
- [49] Xue S, Kwon J, Guo Y, Garg T, Sumption M D and Collings E W 2023 Compressive stress-strain behavior of REBCO coated conductors and cables *IEEE Trans. Appl. Supercond.* **33** 1–6
- [50] Shin H-S and Dederick M J 2013 Intrinsic strain effect on critical current in Cu-stabilized GdBCO coated conductor tapes with different substrates *Supercond. Sci. Technol.* **26** 055005
- [51] Pierro F, Delgado M, Chiesa L, Wang X and Prestemon S O 2019 Measurements of the strain dependence of critical current of commercial REBCO tapes at 15 T between 4.2 and 40 K for high field magnets *IEEE Trans. Appl. Supercond.* **29** 1–5
- [52] Fry V, Estrada J, Michael P C, Salazar E E, Vieira R F and Hartwig Z S 2022 Simultaneous transverse loading and axial strain for REBCO cable tests in the SULTAN facility *Supercond. Sci. Technol.* **35** 075007
- [53] Martovetsky N N et al 2010 Iter central solenoid coil insulation qualification *AIP Conf. Proc.* **1219** 135–44
- [54] Reed R P, Walsh R P, Weeks T, McCloskey J D and Martovetsky N N 2013 Compression-fatigue, elastic modulus, and thermal contraction of insulated conduit arrays of ITER CS modules *IEEE Trans. Appl. Supercond.* **23** 4200805
- [55] Reed R P and Martovetsky N N 2014 Electrical insulation systems for the ITER CS modules *AIP Conf. Proc.* **1574** 354–61
- [56] McLaughlin R E (The American Society of Mechanical Engineers) 2021 Protection against cyclic loading *ASME Boiler and Pressure Vessel Code* vol Sec VIII (Library of Congress) pp 685–90
- [57] Mitchell N 2009 Magnet superconducting and electrical design criteria
- [58] Zichy J and Vecsey G 1987 Design and testing results of the swiss LCT coil *IEEE Trans. Magn.* **23** 819–25
- [59] Hoenig M O and Montgomery D B 1975 Dense supercritical-helium cooled superconductors for large high field stabilized magnets *IEEE Trans. Magn.* **11** 569–72
- [60] Mitchell N 2007 Assessment of conductor degradation in the ITER CS insert coil and implications for the ITER conductors *Supercond. Sci. Technol.* **20** 25
- [61] Hubbard A et al Processes, systems and devices for metal filling of high temperature superconductor cables *WO2021097049A1* (available at: <https://patents.google.com/patent/WO2021097049A1/en>)
- [62] Sgobba S 2020 Vacuum for accelerators: introduction to materials and properties (arXiv:2006.02212)
- [63] Viebke H, Gustke D, Rummel T, Sborchia C, Schroeder R, Williams D, Bates S, Leigh B and Winter R 2006 Lessons learned from the manufacture of the W7-X planar coils *J. Phys.: Conf. Ser.* **43** 748
- [64] Nuclear Newsletter Stress corrosion cracking and welding nonconformities are behind ITER's fresh delays (available at: www.ans.org/news/article-4553/stress-corrosion-cracking-and-welding-nonconformities-are-behind-iters-fresh-delays/) (Accessed December 3 2023)
- [65] Lu J, Xin Y, Jarvis B and Bai H 2021 Oxygen out-diffusion in REBCO coated conductor due to heating *Supercond. Sci. Technol.* **34** 075004
- [66] Pan X, Wu W, Yu X, Lu L, Guo C and Zhao Y 2023 Typical electrical, mechanical, electromechanical characteristics of copper-encapsulated REBCO tapes after processing in temperature under 250 °C *Supercond. Sci. Technol.* **36** 034004
- [67] Bonura M, Cayado P, Konstantopoulou K, Alessandrini M and Senatore C 2022 Heating-induced performance degradation of $\text{REBa}_2\text{Cu}_3\text{O}_{7-x}$ coated conductors: an oxygen out-diffusion scenario with two activation energies *ACS Appl. Electron. Mater.* **4** 1318–26
- [68] Mouratidis T 2022 Low temperature solder demountable joints for non-insulated, high temperature superconducting fusion magnets *Thesis* (Massachusetts Institute of Technology) (available at: <https://dspace.mit.edu/handle/1721.1/147592>) (Accessed April 7 2023)
- [69] Preuss A, Fietz W H, Immel F, Kauffmann-Weiss S and Wolf M J 2018 Critical current degradation of coated conductors under soldering conditions *IEEE Trans. Appl. Supercond.* **28** 1–5
- [70] Martovetsky N N, Berryhill A B and Kenney S J 2012 Qualification of the joints for the ITER central solenoid *IEEE Trans. Appl. Supercond.* **22** 4804004
- [71] Martovetsky N N 2007 Development of the butt joint for the ITER central solenoid *IEEE Trans. Appl. Supercond.* **17** 1358–61
- [72] Michael P C, Gung C-Y, Jayakumar R, Minervini J V and Marzovetsky N N 1999 Qualification of joints for the inner module of the ITER CS model coil *IEEE Trans. Appl. Supercond.* **9** 201–4
- [73] Vasudeva K Demonstration of a REBCO cable joint under high lorentz loads for compact tokamaks *Applied Superconductivity Conf. (Salt Lake City, Utah, USA, 4 September 2024)* (available at: www.appliedsuperconductivity.org/asc2024/)
- [74] Martovetsky N N and Chaplin M R 1996 Normal-zone detection in tokamak superconducting magnets with co-wound voltage sensors *IEEE Trans. Magn.* **32** 2434–7
- [75] Coatanéa M, Duchateau J-L, Lacroix B, Nicolle S, Rodriguez-Mateos F and Topin F 2011 Selection of a quench detection system for the ITER CS magnet *Fusion Eng. Des.* **86** 1418–21
- [76] Hilal M A, Vescey G, Pfotenhauer J M and Kessler F 1994 Quench detection of multiple magnet system *IEEE Trans. Appl. Supercond.* **4** 109–14
- [77] Coatanéa-Gouachet M, Carrillo D, Lee S and Rodríguez-Mateos F 2015 Electromagnetic quench detection in ITER superconducting magnet systems *IEEE Trans. Appl. Supercond.* **25** 1–7
- [78] Chu Y et al 2009 Quench detection based on voltage measurement for the KSTAR superconducting coils *IEEE Trans. Appl. Supercond.* **19** 1565–8
- [79] Murakami H, Kizu K, Tsuchiya K, Kamiya K, Takahashi Y and Yoshida K 2012 Quench detection of fast plasma events for the JT-60SA central solenoid *Fusion Eng. Des.* **87** 23–29
- [80] Martovetsky N N and Radovinsky A L 2014 ITER CS quench detection system and its qualification by numerical modeling *IEEE Trans. Appl. Supercond.* **24** 1–4
- [81] Salazar E E et al 2021 Fiber optic quench detection for large-scale HTS magnets demonstrated on VIPER cable during high-fidelity testing at the SULTAN facility *Supercond. Sci. Technol.* **34** 035027
- [82] Hill K O and Meltz G 1997 Fiber Bragg grating technology fundamentals and overview *J. Light Technol.* **15** 1263–76
- [83] Matveenko V P, Kosheleva N A and Serovaev G S 2022 Strain measurements by FBG-based sensors embedded in various materials manufactured by different technological processes *Proc. Struct. Integr.* **37** 508–16
- [84] Knaster J and Penco R 2012 Paschen tests in superconducting coils: why and how *IEEE Trans. Appl. Supercond.* **22** 9002904
- [85] Khumthong K, Lloyd S, Norausky N, Piec Z, Schaubel K and Smith J 2018 Paschen testing of ITER central solenoid

- qualification module *30th Symposium on Fusion Technology (Giardini Naxos, Sicily, Italy, 17 September 2018)* (available at: <https://agenda.enea.it/event/60/contributions/340/>)
- [86] Davis S 2021 Integrated commissioning status on 09.07.2021 (available at: www.jt60sa.org/)
- [87] Golfinopoulos T *et al* 2024 Building the runway: a new superconducting magnet test facility made for the SPARC toroidal field model coil *IEEE Trans. Appl. Supercond.* **34** 1–16
- [88] Granetz R Calculating the expected DC critical current for HTS VIPER cables and coils *Applied Superconductivity Conf. (Salt Lake City, Utah, USA, 2 September 2024)* (available at: www.appliedsuperconductivity.org/asc2024/)
- [89] Strickland N M, Wimbush S C, Pantoja A, Pooke D M, Fee M, Chamritskii V, Hartwig Z, Cheng J, Garberg S and Sorbom B 2021 Extended-performance ‘supercurrent’ cryogen-free transport critical-current measurement system *IEEE Trans. Appl. Supercond.* **31** 1–5
- [90] Cheng J Quantification of critical current prediction uncertainty in fusion cables introduced by variations in high temperature superconductor datasets *28th Int. Magnet Technology Conf. (Aix-en-Provence, France, 14 September 2023)* (available at: <https://mt28-aoscongres.com/>)